Pax2a regulates angiogenesis to facilitate fusion of the optic fissure

Megan L. Weaver[1], Piedade. W. P[1], Meshram, N.N[1] and J.K. Famulski[1].

1. Department of Biology, University of Kentucky

Key Words: Optic Fissure, coloboma, pax2, choroid fissure, hyaloid vasculature, anti-angiogenesis

ABSTRACT:

Formation of the vertebrate retina involves timely and precise fusion of the optic fissure, failure of which results in the congenital blinding disorder coloboma. The optic fissure forms in consequence of optic cup morphogenesis and has a functional role as a conduit for migration of endothelial vasculature during hyaloid vasculogenesis. Recent studies have linked hyaloid vasculature precursor cells to be potential triggers, initiating optic fissure fusion. In order to examine this link, we analyzed the molecular events associated with optic fissure fusion and hyaloid vasculogenesis in the zebrafish pax2a mutant coloboma model. By means of wholemount immunohistochemistry, we determined that optic fissure fusion initiation, as indicated by laminin remodeling, is preceded by a spike in F-actin signaling. In contrast, the spike in F-actin activity and the disassembly of the basement membrane (BM) were misregulated in pax2a$^{-/-}$ embryos. To examine how the fusion process is disrupted in the absence of pax2a function, we compared transcriptomic profiles between pax2a$^{-/-}$ and wildtype (WT) embryos. This analysis uncovered a novel connection between regulation of angiogenesis and fusion. Loss of pax2a function resulted in significant reduction of talin1 expression, a known regulator of endothelial vasculature migration associated with fissure fusion. In addition, loss of pax2a also resulted in increased expression of an anti-angiogenic protease, ADAMTS1. 3D confocal and live imaging of retinal hyaloid vascularization in Tg[kdrl:mCherry] embryos indicated a significant deficit in pax2a$^{-/-}$ embryos while pharmacological inhibition of VEGF using DMH4 or ADAMTS1 mRNA overexpression phenocopied the pax2a mutant phenotype. Taken together, we propose that Pax2a positively regulates tln1 while negatively regulating ADAMTS1 expression. This enables timely hyaloid vascularization of the retina which in turn directly signals to initiate fissure fusion via cytoskeletal rearrangements and subsequent BM remodelling.

AUTHOR SUMMARY

Formation of a fully functioning human eye requires precise and coordinated cellular mechanisms during very early development. One such mechanism is responsible for the formation of the eyeball structure from a flat sheet of cells to a hemispherical organ. In order to facilitate the biophysical properties of this shape change, an opening on the ventral side of the eye forms and must be closed in order to properly form the eyeball. Failure of this event leads to pediatric blindness in the form of a disease termed Coloboma. While it has been studied by researchers for almost a century, we still lack a significant understanding of how and why some children are born with this disease. In this study, we aimed to better understand how the closure of this opening is triggered by the developing tissues. What we found is, that non-eye cells which are found within this opening and are making vasculature networks to nourish the eye, are likely triggers for the fusion event. We found that regulating their migration and proliferation, also known as angiogenesis, is required for closure of this opening and therefore proper development of the eye.

82 **INTRODUCTION:**

83 Ocular development is a highly conserved process amongst vertebrate species.
84 Assembly of the hemispherical retinal structure from an initially flat sheet of cells
85 requires many complex morphogenetic movements. One such morphogenetic
86 movement involves the invagination of the optic vesicle which results in a fissure
87 forming at the ventral region of the developing retina. This fissure, known as the choroid
88 or optic fissure (OF), enables hyaloid vasculature endothelial cell migration into the
89 developing retina and subsequent establishment of the hyaloid vasculature. Hyaloid
90 vasculature is a temporary circulatory system required for ocular development, and in
91 most cases will degenerate once mature blood vessels begin to grow (1-4). As soon as
92 the hyaloid vasculature has been established, the two opposing retinal epithelial sheets
93 of the optic fissure will undergo fusion. Thereby, they encase the ganglion cell axons
94 localized in the optic stalk and complete retinal morphogenesis. Failure of OF fusion
95 leads to a congenital blinding disorder known as coloboma (5-7). Coloboma is a
96 prevalent cause of pediatric blindness, accounting for approximately 10% of cases
97 worldwide (6, 8). This makes it one of the leading causes of pediatric blindness.
98 Coloboma is a spectrum disorder presenting unilaterally or bilaterally and ranging in
99 severity from minor visual impairment, to complete blindness in the affected eye (9).
100 This spectrum of severity is associated with the location and degree to which the
101 choroid fissure was able to fuse and the severity of subsequent loss of ganglion cell
102 axons (7). The process of epithelial tissue fusion is not unique to the eye and occurs
103 throughout development, encompassing neural tube closure, palatal shelf formation and
104 eyelid development to name a few. Similar to the failure of optic fissure fusion,
105 congenital disorders have been associated with various organs where epithelial fusion
106 fails (10). Epithelial fusion has been studied for over a century, and is known to involve
107 transcriptional regulation, cell signaling pathways, and morphogen gradients (11, 12).
108 However, in regard to the optic fissure we are still lacking a basic understanding of how
109 these molecular mechanisms coordinate and directly facilitate fusion. Recent work has
110 begun to implicate some of the cellular processes involved in optic fissure fusion. For
111 example, the actin cytoskeleton is known to be a crucial component of the machinery
112 driving fusion of the optic fissure as well as other tissues (13). The importance of the

113 actin cytoskeleton during epithelial fusion is thought to involve lamellipodia and filopodia
114 projections between the two opposing epithelia. These help to “zipper” the cells together
115 to form a single continuous sheet. When lamellipodial and filopodial projections are
116 precluded, fusion often fails (14). Interestingly, these projections were observed during
117 OF fusion almost 3 decades ago (15-17). However, while it has been observed that
118 actin protrusions likely play a functional role during OF fusion, it still remains to be
119 determined what signals rearrangement of the actin cytoskeleton. The second cellular
120 mechanism known to be directly involved in epithelial fusion is the remodeling of the
121 basement membrane (BM). During epithelial fusion, the BM acts as a physical barrier
122 restricting the establishment of cell to cell contacts, which must be removed in order for
123 fusion to complete. Recent work, including our own, across several species has
124 characterized progressive removal of the BM during choroid fissure fusion (18, 19).
125 However, the molecular mechanisms facilitating this process, in particular BM
126 remodeling, remain largely unknown. It was recently shown that migrating hyaloid
127 vasculature precursors found in the OF could potentially signal BM remodeling in
128 anticipation of fusion (19). James *et al.* 2016, showed that mutations in zebrafish talin1,
129 an actin cytoskeleton scaffolding protein known to be required for endothelial cell
130 migration (20), result in choroid fissure fusion defects. Theirs, and previous studies also
131 indicated that *cloche* mutants, which lack all early hyaloid vasculature, have delayed
132 basement membrane breakdown in the region of the choroid fissure (19, 21). Hyaloid
133 vasculature has long been a hypothesized to be an initiating factor of optic fissure
134 fusion. It’s role during retinal development is to establish a vasculature supply to the
135 developing retina and lens while connecting to the choroid vasculature for proper blood
136 flow (3). Hyaloid vasculogenesis takes advantage of an open optic fissure so that
137 vasculature cells can migrate into the developing optic cup. Once optic fissure fusion is
138 completed, hyaloid vasculature is fully established. It has therefore been proposed that
139 because hyaloid vasculature requires an open fissure to complete establishment of its
140 network, migrating hyaloid vasculature cells could directly signal to the opposing retinal
141 lobes and regulate the timing of fissure fusion. This mechanism could potentially involve
142 vasculature-mediated activation of the fusion machinery within the retinal rim cells, or
143 direct supply of molecular factors, such as matrix proteases (22). In additional support

144 of this hypothesis, recent optic cup transplantation experiments in zebrafish embryos
145 confirm that in the absence of hyaloid vasculature, ectopic retinal OFs fail to initiate
146 fusion (23). There is therefore a clear link between OF fusion initiation and hyaloid
147 vasculature migration through the fissure.
148
149 Coloboma has been studied for many decades in many different species. This
150 has led to a general outline of the signaling and morphogenetic pathways required for
151 proper OF formation and fusion (recently reviewed in (24)). In particular, opposing
152 action of bone morphogenetic protein (BMP) and sonic hedgehog (Shh) signaling
153 establishes the dorso-ventral pattern of the optic vesicle and ensures proper expression
154 of optic stalk and OF regulators pax2, vax1 and vax2 (25, 26). However, as outlined
155 above, the actual molecular mechanisms driving the fusion process remain largely
156 unknown. Recent work from our lab has begun to decipher the composition and timing
157 of remodeling of the OF BM (27), however, the field still lacks a detailed understanding
158 of the cellular processes during and leading up to OF fusion. Hence, we have
159 undertaken a detailed analysis of zebrafish OF fusion comparing WT and the pax2a$^{-/-}$
160 coloboma model (28). In particular we have characterized the timing of BM remodeling,
161 F-actin dynamics, morphological apposition and hyaloid vascularization. Furthermore,
162 using transcriptomic analysis to compare WT and pax2a$^{-/-}$ eyes we discovered
163 misregulation in angiogenic signaling, resulting in decreased vasculogenesis of the
164 early retina and OF fusion failure. In particular we found that pax2a$^{-/-}$ embryos exhibit a
165 decrease in talin1 expression coupled with an increase in *A disintegrin and*
166 *metalloproteinase with thrombospondin motifs 1 (*ADAMTS1) expression, an anti-
167 angiogenic protease (29, 30). Modulation of vascularization via pharmacological
168 inhibition of VEGF signaling or overexpression of ADAMTS1 both phenocopied the
169 pax2a$^{-/-}$ hyaloid vasculature and coloboma phenotypes. This has led us to propose a
170 novel pathway for the regulation of optic fissure fusion where pax2a mediates proper
171 regulation of anti-angiogenic factors in order to facilitate hyaloid vasculature migration
172 through the OF. Timely migration of hyaloid vasculature cells in turn signals to the retina
173 rim cells, via F-actin, and initiates the fissure fusion machinery, in particular remodeling
174 of the BM.

175

176 **RESULTS:**

177

178 **<u>Optic Fissure basement membrane remodeling is preceded by F-actin signaling.</u>**

179 Several recent studies have undertaken a detailed time course to map out the
180 exact timing of optic fissure fusion in numerous species, including zebrafish (18, 19).
181 Overall, in zebrafish, the data point to ~32-36hpf as the time of OF fusion initiation,
182 observed by BM remodeling. To better understand the molecular mechanisms
183 regulating OF fusion, we also performed a detailed time course analysis of OF BM
184 remodeling, using laminin immunohistochemistry (IHC) as a read out of this process.
185 We performed whole mount IHC for laminin deposition in embryos starting at 24hpf and
186 sampling every 4 hours up to 48hpf and then at 56 and 72hpf (Fig 1A). To analyze the
187 progression of the fusion process, we quantified the laminin signal within the OF from
188 3D z-stacks of confocal scans. Regions of the BM outside the OF and juxtaposed to the
189 developing lens were used to normalize the laminin signal (Fig S1A). In particular we
190 quantified laminin signal in the central proximal region of the fissure (Fig S1B). This
191 region has been shown to represent the site of fusion initiation. In agreement with
192 recent studies in zebrafish, we found that OF fusion initiates at ~32-36hpf and does so
193 in a central region of the fissure, subsequently proceeding proximally and distally (Fig
194 1B). By 48hpf, we observed most of the laminin signal is removed from the OF, and by
195 72hpf, little to no laminin persists in the region (Fig 1A, B). In addition to examining the
196 timing of OF BM remodeling, we also determined whether changes in F-actin dynamics
197 correlate to the timing of fissure fusion. James *et al*, 2016 had recently suggested that
198 infiltrating vasculature endothelial cells migrating through the fissure could be a source
199 of signal for fissure fusion. In fact, they showed that vasculature cell interaction with the
200 fissure results in an increase of cytoskeletal, F-actin, rearrangements (19). To track F-
201 actin signaling during fusion we stained the laminin labeled embryos using phalloidin
202 and quantified the signal within the fissure. To normalize staining intensity we used an
203 interior region of the retina (Fig S1A). Our analysis revealed a spike in OF associated
204 F-actin signal between 24-32hpf, preceding the time that BM remodeling is initiated (Fig
205 1A,B). We also noticed a second spike of F-actin activity around 44hpf, a time of active

206 fusion (Fig 1C). Interestingly, the observed spikes in F-actin activity correlate with the
207 timing of hyaloid vasculature migration (24-32hpf) through the fissure and the expected
208 timing of actin protrusions facilitating epithelial fusion (36-48hpf). When measuring
209 distance between the fusing lobes of the retina we observed apposition to complete
210 around 36-40hpf (Fig S2). Taken together, we concluded that both apposition and BM
211 remodeling are preceded by a spike in F-actin within the OF driving initiation of BM
212 remodeling and subsequently fusion.
213
214 **Optic fissure fusion mechanics are altered and disrupted upon loss of Pax2a**
215 **function.**
216 In order to test our theory that an F-actin signaling wave precedes and drives
217 subsequent OF fusion we compared our findings to an established model of coloboma,
218 the pax2a^{noi} line (28). Pax2 is a critical regulator of OF fusion in several model systems
219 and has been documented in human coloboma cases (31-33). The noi mutation is
220 predicted to result in a loss of Pax2a function due to a premature stop codon at position
221 198 (34). Originally characterized for their no-isthmus phenotype, pax2a$^{noi/noi}$ embryos
222 (referred to as pax2a$^{-/-}$ from this point on) elicit a fully penetrant unfused OF in addition
223 to severe heart defects. Unfortunately, homozygotes are not viable and do not enable
224 the study of coloboma at juvenile or adult stages. We hypothesized that examining the
225 molecular events leading to OF fusion in the pax2a^{noi} system would inform us whether
226 these events are functionally important. Similar to our WT study, we examined lobe
227 distance, in addition to laminin and F-actin levels throughout the time OF fusion (Fig 2A,
228 Fig S1C). In stark contrast to WT, pax2a$^{-/-}$ embryos did not exhibit a significant decrease
229 in laminin signal between 32-48hpf, in fact, laminin appears to be largely retained in the
230 OF of pax2a$^{-/-}$ embryos (Fig 2B). While there is moderate decrease in laminin signal in
231 pax2a$^{-/-}$ embryos from 32-36hpf, this is well above the levels observed in WT. IHC
232 images clearly show that laminin persists in the fissure up to and including 72hpf (Fig
233 2A). A time when WT OF fusion is already completed and clearly absent of laminin
234 signal (Fig 1A). When examining F-actin levels in pax2a$^{-/-}$ embryos we did not detect a
235 spike in activity between 24 and 32hpf. Also, F-actin levels fluctuate between 36 and
236 44hpf and finally drop to WT levels by 48hpf. As such, it appears the absence of F-actin

signaling at early timepoints, 24-32hpf, correlates with failure to initiate fusion. Lastly, when examining retinal lobe distance in pax2a$^{-/-}$ embryos we do not observe any significant defects in apposition (Fig S2). Taken together, we conclude that in the absence of pax2a the molecular mechanism regulating OF fusion, likely involving F-actin signaling, fails to initiate. This is apparent by the persistence of OF BMs. While neither F-actin signaling or BM remodeling is not initiated in pax2a$^{-/-}$ embryos, apposition of the lobes appears largely unaffected indicating that pax2a does not regulate morphogenetic movements of the retinal lobes. Based on these data we propose that the F-actin signaling spike we observe just prior to initiation of OF BM remodeling, in conjunction with pax2a activity, is critical for the completion of OF fusion.

Pax2a retinal transcriptomic profile during optic fissure fusion.

Interestingly, although pax2a has been the subject of intensive research, there are currently no obvious transcriptional targets of pax2a that would directly point to mechanistic regulation of OF fusion. In an effort to understand the absence of OF BM remodeling and misregulation of F-actin activity observed in pax2a$^{-/-}$ embryos we compared retinal transcriptomic profiles between WT and pax2a$^{-/-}$ embryos. Whole retinas from 48hpf WT and pax2a$^{-/-}$ embryos were isolated and total RNA was subsequently purified and sequenced using Illumina sequencing. 48hpf was chosen for our experimental time point as pax2a$^{-/-}$ embryos are easily phenotyped at this age due to severe heart malformation. When comparing three replicates for WT and pax2a$^{-/-}$ embryos using RSEM software, we detected 1215 transcripts significantly upregulated (>95% confidence interval) and 1202 transcripts significantly downregulated (Fig 3A and 3D). Gene ontology analysis indicated a wide spread of biological function being affected, including cytoskeletal signaling, adhesion and developmental processes for both down and upregulated genes (Fig 3B, E). In fact, the distribution of biological function between up and downregulated genes was highly similar (Fig 3B, D). A list of top 20 up and down regulated genes is outlined in Figure 3C and F. Results of all the statistically significant up and downregulated genes identified in our assay are presented as supplementary data (Table 1).

267 From our analysis of downregulated targets, one, talin1 (tln1), stood out in
268 particular. As outlined in the introduction, tln1 was recently shown to be involved in the
269 migration of vasculature endothelial cells and subsequently fusion of the OF (19). As
270 such, we next sought to investigate the relationship between pax2a, tln1,
271 vasculogenesis and optic fissure fusion mechanics.
272
273 **Loss of pax2a function leads to a reduction of hyaloid vasculature migration into**
274 **the optic fissure.**
275 Tln1 has recently been shown to play a role in optic fissure fusion and our
276 discovery of reduced tln1 expression in pax2a$^{-/-}$ retinas engaged us to evaluate this
277 connection further. To validate our RNAseq data, we performed wholemount *in situ*
278 hybridization (WISH) for tln1 comparing WT siblings to pax2a$^{-/-}$ mutant embryos. WT
279 expression of tln1 was observed in the optic fissure between 28 and 48hpf coinciding
280 with pax2a expression (Fig 4A, Fig S3). In pax2a$^{-/-}$ embryos, OF tln1 expression
281 appears significantly reduced compared to WT while retaining similar expression in
282 periocular regions (Fig 4A). Tln1 expression is also reduced in the mid brain-hind brain
283 boundary, another region of strong pax2a expression (Fig 4A, S3A). To determine
284 whether the reduction of tln1 expression in pax2a$^{-/-}$ embryos had functional
285 consequences on optic fissure fusion and hyaloid vasculogenesis we examined pax2a$^{-/-}$
286 embryos expressing mCherry in vasculature cell, Tg[kdrl:mCherry]. Using 3D *in vivo*
287 time-lapse confocal microscopy we recorded migration of mCherry expressing cells
288 through the OF from 24 to 30hpf (Fig 4B, Movie 1). Both WT and pax2a$^{-/-}$ embryos
289 contain vasculature endothelial cells within the fissure at 24hpf, however, over the next
290 6 hours of imaging it becomes clear that a higher number of mCherry expressing cells
291 migrate through the OF in WT than in pax2a$^{-/-}$ embryos (Fig 4B, Movie 1). To quantify
292 this effect, we processed WT and pax2a$^{-/-}$ Tg[kdrl:mCherry] embryos at 24, 32, 36 and
293 48hpf, collected 3D confocal stacks and counted the number of mCherry positive cells
294 found within the fissure (Fig 4C). The data clearly indicate that there is a significant
295 reduction in the number of kdrl:mCherry cells found within the pax2a$^{-/-}$ optic fissure at
296 both 32 and 36hpf (Fig 4D). Furthermore, using 3D rendering rotation, we observed that
297 in 48hpf pax2a$^{-/-}$ embryos the hyaloid vasculature established in the back of the lens is

298 reduced in size and lacks the proper connections to the newly forming choroidal and
299 superficial vasculature systems (Movie 2-3). Overall, our data indicate that loss of pax2a
300 function leads to a decreased and impaired migration of hyaloid vasculature endothelial
301 cells into the optic fissure. Ultimately leading to a disorganized and reduced hyaloid
302 vasculature.
303
304 **Inhibition of VEGF signaling impair optic fissure fusion.**
305 Based on our discovery of reduced hyaloid vasculature in pax2a$^{-/-}$ embryos, we
306 next sought to examine whether this phenomenon is associated with failure of optic
307 fissure fusion. To do so, we turned our attention to vascular endothelial growth factor
308 (VEGF) signaling. VEGF, the ligand for vascular endothelial growth factor receptor
309 (VEGFR), is an angiogenic factor and the prime candidate for signaling the migration
310 and proliferation of hyaloid vasculature endothelial cells in the optic fissure. To inhibit
311 VEGF signaling, we took advantage of the dorsomorphin derivative DMH4, which has
312 been shown to selectively inhibit VEGF signaling independent from BMP (35). Based on
313 previously published working concentrations, we conducted a dose response to
314 examine DHM4 effects on hyaloid vasculature formation using Tg[kdrl:mCherry] as a
315 readout. Treatment of embryos from 12-24hpf, ranging from 1-100μM, resulted in a
316 dose response of reduction of mCherry signal in the developing retina (Fig S4). We
317 decided to use the 100μM concentration for subsequent experiments as this
318 concentration was able to completely inhibit vascularization of the retina up to 72hpf
319 (Fig 5A). Embryos were treated starting at 12hpf and examined for fissure fusion status
320 via whole mount laminin IHC at 24, 32, 36, 48, 56 and 72hpf (Fig 5B). 3D confocal
321 imaging revealed a persistence of laminin signal within the fissure up and including
322 72hpf (Fig 5B) upon DMH4 treatment. Measurement of the laminin signal over our time
323 course generated very similar results to what we observed in pax2a$^{-/-}$ embryos, with
324 laminin persisting within the OF at timepoints where WT embryos have completed
325 remodeling (Fig 5C). In addition to laminin, we also quantified F-actin activity during the
326 treatment (Fig 5B). Again, similar to pax2a$^{-/-}$ embryos we did not observe a spike in F-
327 actin activity between 24-32hpf as observed in WT embryos (Fig 5D). Similar to pax2a$^{-/-}$
328 embryos, DMH4 treatment also did not affect the size of the retina nor the apposition of

329 retinal lobes (Fig S2). Based on these findings, we conclude that inhibition of VEGF
330 signaling results in failure of basement membrane breakdown, presumably due to the
331 absence of vasculature endothelial cell migration through the optic fissure. This is
332 further supported by a lack of increased F-actin signaling during the time of vasculature
333 migration through the OF. As such, our results give direct evidence for the necessity of
334 vasculature endothelial cell migration through the OF in order to initiate BM remodeling
335 and ultimately achieve fusion of the fissure.
336
337 **Pax2a negatively regulates ADAMTS1 expression to inhibit anti-angiogenesis.**
338 Having established a clear connection between pax2a function and proper
339 recruitment of hyaloid vasculature endothelial cells into the optic fissure, we sought to
340 examine the mechanisms behind this phenotype. Our transcriptomic comparison of WT
341 and pax2a$^{-/-}$ eyes, with a focus on angiogenesis regulation, revealed misexpression of *a*
342 *disintegrin and metalloproteinase with thrombospondin motifs 1* (ADAMTS1), a secreted
343 protease known to be involved in regulating VEGF signaling (36). Being a member of
344 the ADAMTS family, ADAMTS1 encodes three thrombospondin motifs enabling it to
345 directly bind and sequester VEGF (30). Furthermore, the protease activity of ADAMTS1
346 has bene shown to target *thrombospondin* (thsb) 1 and 2 for cleavage, ultimately
347 liberating their active forms of which bind to and block VEGF from binding the VEGF
348 receptor (29). In our transcriptomic comparison we found that ADAMTS1 expression
349 was upregulated almost two-fold in pax2a$^{-/-}$ retinas. This would suggest that the
350 expression of ADAMTS1, and therefore its anti-angiogenic activity, is normally
351 somehow kept in check by pax2a. Pax2a has not been reported to harbor
352 transcriptionally repressive function, so this may involve an indirect mechanism. To
353 confirm our RNAseq results we performed WISH, examining ADAMTS1 expression at
354 28 and 36 hpf. In agreement with our transcriptomic analysis, we observed an
355 upregulation in ADAMTS1 in eyes of pax2a$^{-/-}$ embryos, specifically in the region of the
356 optic fissure (Fig 6A). To test whether upregulation of ADAMTS1 expression would have
357 direct effects on hyaloid vasculature migration and optic fissure fusion we injected
358 Tg[kdrl:mCherry] expressing embryos with 100pg ADAMTS1 mRNA. We subsequently
359 examined hyaloid vasculature using 3D confocal imaging between 24-48hpf. Injection of

360 ADAMTS1 mRNA resulted in a significant decrease in the number of kdrl:mCherry cells
361 found within the optic fissure (Fig 6B, Movie 5). Quantification of mCherry positive cells
362 within the optic fissure confirmed this observation (Fig 6C). The reduction in the
363 numbers of mCherry positive cells within the fissure was similar to what we observed in
364 pax2a$^{-/-}$ embryos (Fig 4, Movies 2, 5). This result indicated that the anti-angiogenic
365 function of ADAMTS1 applies to regulating hyaloid vasculogenesis. In contrast to
366 ADAMTS1 mRNA overexpression, we also examined the consequences of ADAMTS1
367 loss of function using morpholino-mediated transient knockdown of ADAMTS1.
368 Tg[kdrl:mCherry] expressing embryos injected with ADAMTS1 morpholinos had a
369 contrasting phenotype to that of pax2a$^{-/-}$ or ADAMTS1 mRNA injected embryos.
370 Morphant ocular vasculature appeared expanded and significantly disorganized, in
371 particular within the dorsal regions (Fig 6D, Movie 6). Morphants did not display any
372 distinct phenotypes in hyaloid vasculature of the optic fissure at 48hpf, however, we did
373 note improper connections being formed as well as a disorganization of the dorsal
374 vasculature network as compared to WT (Fig 6D and Movies 4,6). These findings
375 suggest that while ADAMTS1 activity needs to be suppressed in the optic fissure, other
376 regions of the retinal vasculature may rely on proper levels of ADAMTS1 to enact
377 proper connections within the hyaloid/choroidal network.
378
379 **Misregulation of ADAMTS1 expression leads to optic fissure fusion failure**
380 Having mimicked the vasculature phenotype of pax2a mutants, we next
381 examined whether overexpression of ADAMTS1 would also inhibit optic fissure fusion.
382 To do so, we performed whole mount laminin and F-actin IHC in ADAMTS1 mRNA
383 injected embryos at 24, 32, 36, 48 and 72hpf (Fig 7A). Confocal imaging of the fissure
384 indicated that like the vasculature phenotype, ADAMTS1 mRNA injection also
385 phenocopied pax2a$^{-/-}$ associated persistence of laminin and therefore failure of optic
386 fissure fusion (Fig 7B). Levels of laminin persisting at 48hpf was similar to pax2a$^{-/-}$
387 embryos. As was observed with pax2a$^{-/-}$, timing for apposition of the lobes was not
388 affected in ADAMTS1 overexpressing embryos. Furthermore, as documented for
389 pax2a$^{-/-}$ and DMH4 treated embryos, we again noted a lack of the F-actin signaling
390 spike between 24-32hpf, and no significant difference to WT levels by 48hpf (Fig 7C).

391 Maintaining proper levels of ADAMTS1 expression is therefore necessary to ensure
392 timely fusion of the fissure. Taken together, we envision that pax2a functions to restrict
393 expression of ADAMTS1 within the optic fissure to ensure proper recruitment and
394 migration of hyaloid vasculature endothelial cells. One established, the hyaloid
395 vasculature in turn signals to the retinal rim cells to initiate BM remodeling and leads to
396 subsequent OF fusion.
397
398 **DISCUSSION**
399 Pax2 is the best recognized regulator of optic fissure fusion with a direct
400 connection to pediatric cases of coloboma. Interestingly, while the association of pax2
401 and coloboma is undoubted, little molecular detail exists of how pax2 actually confers
402 this important function. At the same time, studies of optic fissure fusion dating back
403 several decades have been suggesting a direct connection between the fusion process
404 and migrating vasculature endothelial, or periocular mesenchyme, cells found within the
405 fissure prior to and during fusion. A notion strongly supported by recent findings where
406 reduction of hyaloid vasculature in the fissure, or removal of optic vesicles from sources
407 of vasculature inhibits or significantly delays fusion (19, 23). In our study, we outline a
408 novel connection between pax2a function and hyaloid vasculature-mediated initiation of
409 optic fissure fusion, further strengthening the hypothesis that vasculature directly signals
410 initiation of fissure fusion.
411
412 Several recent reports, including this one, have comprehensively characterized
413 optic fissure fusion timing. Work from zebrafish, mice and chick all point to an orderly
414 progression involving: **1)** retinal growth and cellular rearrangement leading to nasal and
415 temporal retinal lobe apposition, **2)** invasion of the fissure by endothelial and neural
416 crest cells forming the hyaloid vasculature system, **3)** cellular signaling, either between
417 retinal rim cells or between rim cells and the migrating vasculature cells, likely in the
418 form of cytoskeletal activation (f-actin), **4)** remodeling or removal of the basement
419 membrane to enable physical connection of the rim cells and subsequent formation of a
420 continuous retinal epithelial sheet via re-polarization and cell-cell adhesion. Step 1 has
421 been nicely characterized in a few recent publications outlining the flow of retinal cells

422 and morphological formation of the fissure (37-39). For step 2, several reports have
423 carefully characterized the formation of the hyaloid vasculature system, including
424 migration of hyaloid vasculature precursor cells into the fissure as soon as it forms (1-3).
425 Importantly, perturbation of this process, or removal of the developing eye from its
426 source, has been shown to lead to fissure fusion failure (19, 23). To date, steps 3 and 4
427 are the least well understood. Several molecular components associated with cell-cell
428 adhesion and epithelial sheet fusion have been associated with the fissure, including α-
429 catenin, n-cadherin, and netrin (19, 40-43). However, the timing or the molecular
430 mechanism organizing and regulating these components remain uncharacterized.
431 Furthermore, very little information exists pertaining to the identity of protease enzymes
432 responsible for BM remodeling. Recent work from our lab has characterized the
433 composition of core BM components within the fissure, but to date, only ADAM16 has
434 been functionally examined in context of fissure fusion, while MMP2 was detected
435 during fusion in mice and MMP23bb implicated from transcriptomic comparison of pre
436 and post fusion fissure expression (42, 44, 45). Identifying proteases active in OF fusion
437 continues to be an area of needed attention. In our current study, we attempted to
438 address the questions of step 3 by concurrently analyzing f-actin and BM remodeling. In
439 doing so we discovered that BM remodeling is preceded by an uptick in F-actin
440 signaling. The timing of this coincides with the active migration of hyaloid vasculature
441 precursors through the fissure. An event shown previously to involve in F-actin signaling
442 within in the fissure (19). Furthermore, we show both genetically and pharmacologically
443 that hyaloid vasculature precursors are necessary for OF fusion, and ultimately outline a
444 mechanism where suppression of anti-angiogenic activity within the fissure is critical for
445 OF fusion. These findings not only confirm a long-held hypothesis of hyaloid vasculature
446 involvement in OF fusion, but also uncover previously unexplored mechanisms of
447 angiogenesis playing a role in the OF fusion process.
448
449 Based on our IHC time course analysis of optic fissure fusion dynamics, in
450 particular F-actin and laminin status, we propose that BM remodeling is preceded by an
451 increase of F-actin activity. This likely stemming from the interaction of retinal and
452 vasculature cells within the fissure (Fig 1). Interestingly, when examining this process in

453 the pax2a^{noi} mutant line we did not detect an increase of Factin signaling at times
454 preceding fusion. This coincided with a decrease in the number of vasculature cells
455 found within the fissure and ultimately lead to failure of optic fissure basement
456 membrane remodeling and lack of fusion. In an attempt to understand the molecular
457 consequence driving these differences we uncovered misregulation of tln1 expression in
458 the absence of pax2a function. Tln1 is a key regulator of endothelial cell migration
459 recently shown to be directly involved in OF fusion (19). In fact, loss of tln1 function
460 leads to a decrease in fissure associated vasculature and persistence of the OF BM.
461 Our finding that pax2a regulates expression of tln1 has several compelling implications.
462 Talin1 is known to be a direct link between the actin cytoskeleton and the BM via
463 integrin (46, 47). Furthermore, tln1 has been associated with the formation of adhesion
464 junctions and other cell-cell interaction processes (48, 49). One could therefore
465 hypothesize several different models for its role in optic fissure fusion. Our, and
466 previous analyses of tln1 expression do not directly indicate which cells within the
467 fissure are expressing tln1. It could be the retinal lobe rim cells, the migrating
468 vasculature cells or both. As such, we can envision that tln1 could function through
469 differing mechanisms. If expressed solely in the retinal cells, then tln1 may function to
470 act as a sensor for the apposition of retinal lobes, or for the presence, or absence, of
471 vasculature endothelial cells. James et al. 2016 showed that vasculature cells within the
472 fissure trigger F-actin accumulation and presumably cytoskeletal signaling, potentially
473 facilitated by tln1. A feature that is missing in pax2a mutant fissures. Furthermore, tln1
474 may also act as a direct mechanism required for the formation of adhesions between
475 the fusing lobes. However, as observed in both tln1 and pax2 mutants, the BM persists
476 at times fusion should be occurring, suggesting that tln1 first plays a functional role in
477 the initiation of BM remodeling, and it remains unclear whether its directly involved in
478 cell-cell adhesion. Future work will focus on answering these questions.
479
480 Our study clearly supports the notion that vasculature plays an integral part in OF
481 fusion. As such, regulation of angiogenesis may also be part of the mechanism. Using a
482 transcriptomic comparison of WT and pax2a mutants we did in fact discover a
483 connection between angiogenesis and pax2a. In the absence of pax2a function we

484 observe an upregulation of ADAMTS1. Encoding 3 thrombospondin (thsb) motifs able to
485 directly bind and sequester VEGF, in addition to targeting thsb1 and 2 for cleavage into
486 their VEGF inhibitory active forms, ADAMTS1 has been extensively studied anti-
487 angiogenic factor in cancer, aortic and renal biology (50). In fact, we showed that
488 upregulating ADAMTS1 expression partially inhibits hyaloid vasculature migration into
489 the optic fissure, an outcome similarly observed in pax2a^{noi} embryos. Up regulation of
490 ADAMTS1 also prevented the F-actin spike and OF BM remodeling while having no
491 effect on eye size or retinal lobe apposition. Along those same lines we also showed
492 that optic fissure fusion and preceding F-actin signaling are abolished when
493 pharmacologically inhibiting VEGF using DHM4. Interestingly, knockdown of ADAMTS1
494 using morpholino resulted in hyaloid vasculature disorganization, suggesting anti-
495 angiogenesis may function to guide and/or shape the developing vasculature network
496 during retinal development. Taken together, our study confirms an undeniable link
497 between hyaloid vasculogenesis and optic fissure fusion. It also uncovers a molecular
498 mechanism involving angiogenic regulation to ensure proper and timely establishment
499 of hyaloid vasculature and subsequent OF fusion.
500

501 **MATERIALS AND METHODS**

502

503 Zebrafish and embryo maintenance

504 Zebrafish were maintained using husbandry procedures approved by University of
505 Kentucky IACUC committee. Embryos were kept at 28.5^{o}C in E3 embryo media. AB and
506 TL strains were used as wild-type, Tg[*kdrl*:mCherry] transgenic line was used to
507 visualize retinal vascularization (51).

508 Pax2^{noi} embryos were a gift from Dr. Gregory-Evans. Genotyping analysis was
509 conducted by amplifying the region of gDNA with the noi mutation using the forward
510 primer: 5'- CTCGCTCTGCCTCCATGATTG3-'and the reverse: 5'-
511 GGCACTGAAAGAGCACAGG -3'. The resultant 460bp amplicon was digested with
512 TaqI (NEB) which would recognize and digest the WT allele sequence but not the
513 mutant allele.

514

515 Immunohistochemistry (IHC)

516 Dechorionated embryos were fixed with 4% PFA in PBS at room temperature for 3h
517 and washed with PBST 4 times for 5 minutes. Embryos were then permeabilized with
518 Proteinase K, 30μg/mL 10 minutes for 24-28 hpf, 50μg/mL 15-20 minutes for 32-48 hpf
519 and 75μg/mL 20 minutes for 56-72 hpf, washed 2 times in PBST for 5 minutes and
520 blocked overnight at 4°C with 10% sheep serum, 0.8% Triton X-100 and 1% BSA in
521 PBS. Primary mouse anti-laminin antibody (ThermoFisher – 1:100) in blocking buffer
522 (1% sheep serum, 1% BSA and 0.8% Triton X-100 in PBS) were incubated overnight at
523 4°C and washed 5 times in PBST for 15 minutes. Secondary antibody, goat anti-rabbit
524 (Alexa Fluor® 488 – Abcam – 1:1000), DAPI 1:1000, and phalloidin (Alexa Fluor® 555 -
525 1:50) were incubated overnight at 4°C in the dark. Tg[*kdrl*:mCherry] embryos were
526 treated with proteinase K as described above and stained with DAPI 1:1000 overnight.
527 The embryos were washed 2 times in PBST for 15 minutes and visualized using a
528 Nikon C2+ confocal microscope equipped with a 40X (1.15NA) water immersion
529 objective. Embryos were embedded in 1.2% low melting point agarose on glass bottom
530 35mm dishes (Fluorodish, World Precision Instruments). Images were captured in steps
531 of 3.5 microns for a total of 31.5 microns using Nikon Elements software. Image

532 adjustment, such as cropping and brightness/contrast was performed using Adobe
533 Photoshop.
534
535 Analysis of Fluorescence signal
536 Fiji software (https://fiji.sc) was used to measure the fluorescence intensity of laminin
537 and phalloidin signal from raw image data. In order to account for variability in staining,
538 normalization values were measured for laminin and actin pixel intensity where an area
539 directly outside of the choroid fissure was measured and a ratio was generated between
540 the two values (Fig S1B). For Tg[krdl:mCherry], 3D reconstructions of the optic fissure
541 were generated and individual cells were counted (from the opening of the OF through
542 the back of the lens).
543
544 Stats
545 Student's t-test was used to compare individual time points. One-way ANOVA was
546 used to analyze across treatments. Graphs are displayed as mean +/- standard
547 deviation. Analysis was performed using Prism8 graphing software (GraphPad).
548
549 Total RNA Sequencing
550 WT and Pax2$^{-/-}$ embryos were dissected and collected at 48 hpf and RNA was
551 extracted from dissected eyes using trizol. Pax2a$^{-/-}$ embryos were phenotyped by
552 distinct heart defects only observed in pax2a$^{-/-}$ embryos, as verified by previous
553 genotyping experiments. Dissected eyes were suspended in 1 mL of trizol and sheared
554 with a 22-gauge needle. Samples were incubated at room temperature for 5 minutes,
555 then 200 μL of chloroform was added and vortexed for 1 minute. Samples were then
556 centrifuged at 12,000 g for 15 minutes at 4℃. Aqueous phase was removed and put into
557 fresh RNAse free tube. 3 μL of Glycoblue was added to samples and vortexed for 5
558 seconds. 500 μL of 100% Isopropanol was then added and vortexed for an additional 10
559 seconds. Samples then were incubated at room temperature for 10 minutes. Samples
560 were then centrifuged at 12,000 g for 10 minutes at 4℃. Supernatant was removed and
561 1 mL of 75% EtOH was added and vortexed for 10 seconds. Samples were then
562 centrifuged at 7,500 g for 5 minutes at 4℃. Supernatant was removed and samples then

563 underwent a pulse centrifugation and any remaining supernatant was removed.
564 Samples were then air-dried for 7 minutes at room temperature under a fume hood. 20
565 μL of RNAse free ddH_2O was added to the samples and mixed until pellet dissolved.
566 Samples were finally incubated at 60℃ for 12 minutes and then stored at -80℃.
567 The RNA then underwent a DNase treatment using the DNA-free Kit. 2 μL of 10X
568 DNaseI Buffer, and 1 μL of rDNaseI was added to the entire 20 μL sample. Samples
569 were incubated at 37℃ for 20 minutes, and then 2 μL of DNase Inactivation Reagent
570 was added. Samples were then incubated at room temperature for 2 minutes, mixing
571 samples 3 times. Samples were centrifuged at 10,000 g for 1.5 minutes. Supernatant
572 was then removed and placed into fresh RNase free tube and stored at -80℃.
573 Purified total RNA was sent to Applied Biological Materials Inc. for Illumina
574 sequencing. Bioinformatic analyses were completed using RSEM. Those transcripts
575 which had a greater than 0.95 posterior probability of being differentially expressed
576 were considered significant. Panther (http://pantherdb.org) was used for gene ontology
577 and pie chart generation.
578
579 Whole-mount in situ hybridization (WISH)
580 Whole-mount in situ hybridization was performed as previously described (52). RNA
581 probes were generated using PCR with T7 promoter sequence and subsequently
582 transcribed [DIG labeled] using T7 polymerase (Roche). Primer sequences were 5'-
583 GAGGGCAAGAGAATTCAGTAC-3' and 5'-
584 TAATACGACTCACTATAGGGCAGATTGCACAAGTTCAGAAG-3' for ADAMTS1, 5'-
585 ATGGATATTCACTGCAAAGCAG-3' and 5'-
586 TAATACGACTCACTATAGGGCTAGTGGCGGTCATAGGCAGTG-3' for pax2a, 5'-
587 GCCACAGCTAAAGCAGTGGCTG-3' and 5'-
588 TAATACGACTCACTATAGGGGTACTGCTGCTGTCGGATCAT-3' for talin 1. Images
589 were captured using a Nikon Digital sight DS-Fi2 camera mounted on a Nikon SZM800
590 stereo scope using Elements software. Dissected eyes from 24, to 72hpf embryos were
591 mounted in 70% glycerol and imaged under DIC using a Nikon TiE compound
592 microscope equipped with a 20X (0.7NA) objective and Elements software. Image

593 adjustment, such as cropping and brightness/contrast was performed using Adobe
594 Photoshop.
595
596 Morpholino Injections
597 Translation blocking Morpholino was obtained from Gene Tools, LLC and used to
598 knock down the expression of ADAMTS1. The morpholino used in this study was:
599 Control MO: 5'-CCTCTTACCTCAGTTACAATTTATA-3', Adamts1: 5'-
600 AGACATTATATTCCTGTCAAGTTCT-3'. 6ng of of ADAMTS1 or control morpholino
601 was injected into 1-2 cell stage embryos.
602
603 Live imaging analysis
604 Live imaging of Tg[kdrl:mCherry] embryos was conducted using a Nikon C2+ confocal
605 microscope equipped with at 20X (0.95NA) water immersion objective. 22 hpf embryos
606 were imbedded in 1.1% low gelling agarose in 1-inch glass bottomed Flourodish cell
607 culture dishes (World Precision Instruments) and covered in embryo media, 3-amino
608 benzoic acidethylester (tricaine) to anaesthetize the embryos and 1-phenyl 2-thiourea
609 (PTU) to inhibit pigmentation. Z-stacks 75μm thick with a step size of 2.5μm were
610 captured over the course of 6 hours at 10 minute intervals. The time lapse data were
611 reconstructed in 3D using Elements software. Image adjustment, such as cropping and
612 brightness/contrast was performed using Adobe Photoshop. After imaging, embryos
613 were removed and genotyped.
614
615 DMH-4 treatment
616 Embryos were incubated in embryo media with 5, 25, 50, or 100 μM of DMH-4 (Sigma
617 Life Science) in DMSO starting at 12hpf. Fresh DHM4 containing media was added
618 every 12hpf for timepoints past 24hpf.
619
620 Cloning and mRNA synthesis.
621 Full coding domain sequences for ADAMTS1 (NCBI reference sequence
622 XM_021475923.1), Pax2a (Ensembl transcript ID: ENSDARG00000028148) were
623 amplified from 24hpf zebrafish cDNA using primers 5'-

624 CATGGATCCATGGATATTCACTGCAAAGCA-3' and 5'-
625 ATGCTCGAGCTAGTGGCGGTCATAGGCAGTG-3' for pax2a, 5'-
626 GCGATCGCATGTCTTTTTTGCGTGTGGTG-3' and 5'-
627 CTCGAGTCAACAGGGAGTCAGATTGC-3' for ADAMTS1, cloned into pGEMT
628 (Promega), digested with AsiSI/XhoI, BamHI/XhoI respectively and subsequently cloned
629 into pCS2+. All constructs were verified by sanger sequencing (Eurofinsgenomics).
630 mRNA was synthesized from linearized pCS2 constructs using SP6 mMessage
631 mMachine kit (Ambion) and purified using YM-50 Microcon columns (Amicon, Millipore).
632
633 Ethics Statement
634 The use of zebrafish in this study was approved by the University of Kentucky IACUC
635 committee, Institutional PHS Assurance #D16-00217 (A3336-01) with a protocol
636 number: 2015-1370.
637
638
639
640 **ACKNOWLEDGEMENTS**
641
642 This work for supported by faculty start-up funds provided to JKF from the department
643 of Biology, University of Kentucky. MLW was supported by the Lyman T Johnson
644 scholarship from the University of Kentucky. PPW was supported by Brazilian National
645 Council for Scientific and Technological Development (CNPq) under grant number
646 202970/2014-0. We thank Dr. Jeramiah Smith for assistance with bioinformatic analysis
647 of our RNAseq data and members of the Famulski lab for helpful discussions.
648

650 **REFERENCES:**

651 1. Hartsock A, Lee C, Arnold V, Gross JM. In vivo analysis of hyaloid vasculature
652 morphogenesis in zebrafish: A role for the lens in maturation and maintenance of the
653 hyaloid. Dev Biol. 2014;394(2):327-39.
654 2. Hashiura T, Kimura E, Fujisawa S, Oikawa S, Nonaka S, Kurosaka D, et al. Live
655 imaging of primary ocular vasculature formation in zebrafish. PLoS One.
656 2017;12(4):e0176456.
657 3. Kaufman R, Weiss O, Sebbagh M, Ravid R, Gibbs-Bar L, Yaniv K, et al.
658 Development and origins of zebrafish ocular vasculature. BMC Dev Biol. 2015;15:18.
659 4. Yoshikawa Y, Yamada T, Tai-Nagara I, Okabe K, Kitagawa Y, Ema M, et al.
660 Developmental regression of hyaloid vasculature is triggered by neurons. J Exp Med.
661 2016;213(7):1175-83.
662 5. AS AL, Gregory-Evans CY, Gregory-Evans K. An update on the genetics of
663 ocular coloboma. Hum Genet. 2019.
664 6. Chang L, Blain D, Bertuzzi S, Brooks BP. Uveal coloboma: clinical and basic
665 science update. Curr Opin Ophthalmol. 2006;17(5):447-70.
666 7. Gregory-Evans CY, Williams MJ, Halford S, Gregory-Evans K. Ocular coloboma:
667 a reassessment in the age of molecular neuroscience. J Med Genet. 2004;41(12):881-
668 91.
669 8. Stoll C, Alembik Y, Dott B, Roth MP. Congenital eye malformations in 212,479
670 consecutive births. Ann Genet. 1997;40(2):122-8.
671 9. Huynh N, Brooks BP. Uveal coloboma. JAMA Ophthalmol. 2013;131(10):1274.
672 10. Ray HJ, Niswander L. Mechanisms of tissue fusion during development.
673 Development. 2012;139(10):1701-11.
674 11. Hayes P, Solon J. Drosophila dorsal closure: An orchestra of forces to zip shut
675 the embryo. Mech Dev. 2017;144(Pt A):2-10.
676 12. Jacinto A, Martinez-Arias A, Martin P. Mechanisms of epithelial fusion and repair.
677 Nat Cell Biol. 2001;3(5):E117-23.
678 13. Vasioukhin V, Bauer C, Yin M, Fuchs E. Directed actin polymerization is the
679 driving force for epithelial cell-cell adhesion. Cell. 2000;100(2):209-19.
680 14. Gumbiner BM. Cell adhesion: the molecular basis of tissue architecture and
681 morphogenesis. Cell. 1996;84(3):345-57.
682 15. Hero I. The optic fissure in the normal and microphthalmic mouse. Exp Eye Res.
683 1989;49(2):229-39.
684 16. Hero I. Optic fissure closure in the normal cinnamon mouse. An ultrastructural
685 study. Invest Ophthalmol Vis Sci. 1990;31(1):197-216.
686 17. Geeraets R. An electron microscopic study of the closure of the optic fissure in
687 the golden hamster. Am J Anat. 1976;145(4):411-31.
688 18. Bernstein CS, Anderson MT, Gohel C, Slater K, Gross JM, Agarwala S. The
689 cellular bases of choroid fissure formation and closure. Dev Biol. 2018;440(2):137-51.
690 19. James A, Lee C, Williams AM, Angileri K, Lathrop KL, Gross JM. The hyaloid
691 vasculature facilitates basement membrane breakdown during choroid fissure closure in
692 the zebrafish eye. Dev Biol. 2016;419(2):262-72.
693 20. Monkley SJ, Kostourou V, Spence L, Petrich B, Coleman S, Ginsberg MH, et al.
694 Endothelial cell talin1 is essential for embryonic angiogenesis. Dev Biol.
695 2011;349(2):494-502.

696 21. Dhakal S, Stevens CB, Sebbagh M, Weiss O, Frey RA, Adamson S, et al.
697 Abnormal retinal development in Cloche mutant zebrafish. Dev Dyn.
698 2015;244(11):1439-55.
699 22. Heissig B, Hattori K, Friedrich M, Rafii S, Werb Z. Angiogenesis: vascular
700 remodeling of the extracellular matrix involves metalloproteinases. Curr Opin Hematol.
701 2003;10(2):136-41.
702 23. Gestri G, Bazin-Lopez N, Scholes C, Wilson SW. Cell Behaviors during Closure
703 of the Choroid Fissure in the Developing Eye. Front Cell Neurosci. 2018;12:42.
704 24. Patel A, Sowden JC. Genes and pathways in optic fissure closure. Semin Cell
705 Dev Biol. 2017.
706 25. Take-uchi M, Clarke JD, Wilson SW. Hedgehog signalling maintains the optic
707 stalk-retinal interface through the regulation of Vax gene activity. Development.
708 2003;130(5):955-68.
709 26. Macdonald R, Wilson SW. Pax proteins and eye development. Curr Opin
710 Neurobiol. 1996;6(1):49-56.
711 27. Carrara N, Weaver M, Piedade WP, Vocking O, Famulski JK. Temporal
712 characterization of optic fissure basement membrane composition suggests nidogen
713 may be an initial target of remodeling. Dev Biol. 2019.
714 28. Macdonald R, Scholes J, Strahle U, Brennan C, Holder N, Brand M, et al. The
715 Pax protein Noi is required for commissural axon pathway formation in the rostral
716 forebrain. Development. 1997;124(12):2397-408.
717 29. Lee NV, Sato M, Annis DS, Loo JA, Wu L, Mosher DF, et al. ADAMTS1 mediates
718 the release of antiangiogenic polypeptides from TSP1 and 2. EMBO J.
719 2006;25(22):5270-83.
720 30. Luque A, Carpizo DR, Iruela-Arispe ML. ADAMTS1/METH1 inhibits endothelial
721 cell proliferation by direct binding and sequestration of VEGF165. J Biol Chem.
722 2003;278(26):23656-65.
723 31. Sanyanusin P, McNoe LA, Sullivan MJ, Weaver RG, Eccles MR. Mutation of
724 PAX2 in two siblings with renal-coloboma syndrome. Hum Mol Genet. 1995;4(11):2183-
725 4.
726 32. Sanyanusin P, Schimmenti LA, McNoe LA, Ward TA, Pierpont ME, Sullivan MJ,
727 et al. Mutation of the PAX2 gene in a family with optic nerve colobomas, renal
728 anomalies and vesicoureteral reflux. Nat Genet. 1995;9(4):358-64.
729 33. Torres M, Gomez-Pardo E, Gruss P. Pax2 contributes to inner ear patterning and
730 optic nerve trajectory. Development. 1996;122(11):3381-91.
731 34. Brand M, Heisenberg CP, Jiang YJ, Beuchle D, Lun K, Furutani-Seiki M, et al.
732 Mutations in zebrafish genes affecting the formation of the boundary between midbrain
733 and hindbrain. Development. 1996;123:179-90.
734 35. Hao J, Ho JN, Lewis JA, Karim KA, Daniels RN, Gentry PR, et al. In vivo
735 structure-activity relationship study of dorsomorphin analogues identifies selective
736 VEGF and BMP inhibitors. ACS Chem Biol. 2010;5(2):245-53.
737 36. Tan Ide A, Ricciardelli C, Russell DL. The metalloproteinase ADAMTS1: a
738 comprehensive review of its role in tumorigenic and metastatic pathways. Int J Cancer.
739 2013;133(10):2263-76.

740 37. Eckert P, Knickmeyer MD, Schutz L, Wittbrodt J, Heermann S. Morphogenesis
741 and axis specification occur in parallel during optic cup and optic fissure formation,
742 differentially modulated by BMP and Wnt. Open Biol. 2019;9(2):180179.
743 38. Heermann S, Schutz L, Lemke S, Krieglstein K, Wittbrodt J. Eye morphogenesis
744 driven by epithelial flow into the optic cup facilitated by modulation of bone
745 morphogenetic protein. Elife. 2015;4.
746 39. Knickmeyer MD, Mateo JL, Eckert P, Roussa E, Rahhal B, Zuniga A, et al.
747 TGFbeta-facilitated optic fissure fusion and the role of bone morphogenetic protein
748 antagonism. Open Biol. 2018;8(3).
749 40. Chen S, Lewis B, Moran A, Xie T. Cadherin-mediated cell adhesion is critical for
750 the closing of the mouse optic fissure. PLoS One. 2012;7(12):e51705.
751 41. Lahrouchi N, George A, Ratbi I, Schneider R, Elalaoui SC, Moosa S, et al.
752 Homozygous frameshift mutations in FAT1 cause a syndrome characterized by
753 colobomatous-microphthalmia, ptosis, nephropathy and syndactyly. Nat Commun.
754 2019;10(1):1180.
755 42. Richardson R, Owen N, Toms M, Young RM, Tracey-White D, Moosajee M.
756 Transcriptome profiling of zebrafish optic fissure fusion. Sci Rep. 2019;9(1):1541.
757 43. Smith R, Huang YT, Tian T, Vojtasova D, Mesalles-Naranjo O, Pollard SM, et al.
758 The Transcription Factor Foxg1 Promotes Optic Fissure Closure in the Mouse by
759 Suppressing Wnt8b in the Nasal Optic Stalk. J Neurosci. 2017;37(33):7975-93.
760 44. Cao M, Ouyang J, Guo J, Lin S, Chen S. Metalloproteinase Adamts16 Is
761 Required for Proper Closure of the Optic Fissure. Invest Ophthalmol Vis Sci.
762 2018;59(3):1167-77.
763 45. Tsuji N, Matsuura T, Narama I, Yoshiki A, Ozaki K. Macrophage-Associated
764 Gelatinase Degrades Basement Membrane at the Optic Fissure Margins During Normal
765 Ocular Development in Mice. Invest Ophthalmol Vis Sci. 2018;59(3):1368-73.
766 46. Anthis NJ, Wegener KL, Ye F, Kim C, Goult BT, Lowe ED, et al. The structure of
767 an integrin/talin complex reveals the basis of inside-out signal transduction. EMBO J.
768 2009;28(22):3623-32.
769 47. Wegener KL, Partridge AW, Han J, Pickford AR, Liddington RC, Ginsberg MH, et
770 al. Structural basis of integrin activation by talin. Cell. 2007;128(1):171-82.
771 48. Calderwood DA, Campbell ID, Critchley DR. Talins and kindlins: partners in
772 integrin-mediated adhesion. Nat Rev Mol Cell Biol. 2013;14(8):503-17.
773 49. Prout M, Damania Z, Soong J, Fristrom D, Fristrom JW. Autosomal mutations
774 affecting adhesion between wing surfaces in Drosophila melanogaster. Genetics.
775 1997;146(1):275-85.
776 50. Boerboom D, Lafond JF, Zheng X, Lapointe E, Mittaz L, Boyer A, et al. Partially
777 redundant functions of Adamts1 and Adamts4 in the perinatal development of the renal
778 medulla. Dev Dyn. 2011;240(7):1806-14.
779 51. Wang Y, Kaiser MS, Larson JD, Nasevicius A, Clark KJ, Wadman SA, et al.
780 Moesin1 and Ve-cadherin are required in endothelial cells during in vivo tubulogenesis.
781 Development. 2010;137(18):3119-28.
782 52. Holly VL, Widen SA, Famulski JK, Waskiewicz AJ. Sfrp1a and Sfrp5 function as
783 positive regulators of Wnt and BMP signaling during early retinal development. Dev Biol.
784 2014;388(2):192-204.
785

786 **FIGURE LEGENDS**

787

788 Figure 1: **An increase in F-actin dynamics precedes laminin remodeling during**
789 **optic fissure fusion.**
790 **A)** Whole mount Immunohistochemistry was used to simultaneously visualize F-actin
791 (red) and laminin (green) during optic fissure fusion, 24-72hpf. Central-proximal sections
792 obtained using confocal imaging were collected and quantified. Scale bar = 50um. **B)**
793 Quantification of laminin signal intensity within the optic fissure, normalized to regions of
794 laminin staining juxtaposed to the lens. Relative pixel intensities are displayed. A green
795 dotted line depicts the trend in laminin intensity over time. ANOVA $p<0.0001$. **C)**
796 Quantification of F-actin signal intensity (phalloidin staining) within the optic fissure,
797 normalized to regions of F-actin signal within the lobe of the retina. Relative pixel
798 intensities are displayed. A red dotted line represents the trend in F-actin intensity over
799 time. ANOVA $p<0.0001$.

800

801 Figure 2: **Pax2 mutant embryos lack F-actin activity increase and laminin**
802 **remodeling within the optic fissure.**
803 **A)** Whole mount Immunohistochemistry was used to simultaneously visualize F-actin
804 (red) and laminin (green) during optic fissure fusion, 24-72hpf, in pax2$^{-/-}$ embryos.
805 Central-proximal sections obtained using confocal imaging were collected and
806 quantified. Scale bar = 50um **B)** Quantification of laminin signal intensity within the optic
807 fissure, normalized to regions of laminin staining juxtaposed to the lens. Relative pixel
808 intensities are displayed. A green dotted line depicts the trend in laminin intensity over
809 time. Blue dotted line represents the trend observed in wildtype embryos. ANOVA
810 $p<0.0001$. **C)** Quantification of F-actin signal intensity (phalloidin staining) within the
811 optic fissure, normalized to regions of F-actin signal within the lobe of the retina.
812 Relative pixel intensities are displayed. A red dotted line represents the trend in F-actin
813 intensity over time. Blue dotted line represents the trend observed in wildtype embryos.
814 ANOVA $p<0.0001$.

815

816

817 Figure 3: **Retinal transcriptomic comparison between WT and pax2a$^{-/-}$.**
818 **A)** Heat map representing transcripts found to be significantly down regulated in pax2a$^{-/-}$
819 embryos. **B)** Gene ontology for pax2a$^{-/-}$ downregulated transcripts. **C)** Top 20
820 downregulated transcripts are outlined in order of fold change. **D)** Heat map
821 representing transcripts found to be significantly upregulated in pax2a$^{-/-}$ embryos. **E)**
822 Gene ontology for pax2a$^{-/-}$ upregulated transcripts. **F)** Top 20 upregulated transcripts
823 are outlined in order of fold change.
824
825 Figure 4: **Pax2a is necessary for tln1 expression and recruitment of vasculature**
826 **into the optic fissure.**
827 **A)** Wholemount in situ hybridization comparing tln1 expression between WT and
828 pax2a$^{-/-}$ embryos at 28 and 32hpf. Tln1 signal within the optic fissure (yellow arrowhead)
829 is clearly reduced in Pax2a$^{-/-}$ embryos (red *). **B)** *In vivo* 4D confocal imaging of
830 Tg[kdrl:mCherry] WT or pax2a$^{-/-}$ embryos. Time lapse series depicting the region of the
831 optic fissure (dotted white lines) and mCherry positive vasculature endothelial cells
832 migrating through the fissure. Compared to WT, pax2a$^{-/-}$ embryos display a reduction in
833 the number of vasculature cells migrating in the fissure from 24-29hpf. Scale bar =
834 10um. **C)** Comparison of WT and pax2a$^{-/-}$ vascularization during optic fissure fusion, 24-
835 48hpf. 3D reconstructions of whole mount Tg[kdrl:mCherry] (red) WT or pax2a$^{-/-}$
836 embryos with DNA stained by DAPI (blue). Scale bar = 50um. **D)** Quantification of
837 mCherry positive cells from 3D confocal stacks within the region of the optic fissure.
838 Individual embryo results are depicted. ANOVA $p<0.0001$.
839
840 Figure 5: **Inhibiting angiogenesis prevents optic fissure fusion.**
841 **A)** 3D confocal imaging of Tg[kdrl:mCherry] (red) embryos treated with DMH4 at 24-
842 72hpf. DNA was stained with DAPI (blue). Scale bar = 50um. DMH4 treatment restricts
843 the migration of vasculature endothelial cells into the fissure and retina. **B)** Whole mount
844 Immunohistochemistry was used to simultaneously visualize F-actin (red) and laminin
845 (green) in DMH4 treated embryos during the time of optic fissure fusion, 24-72hpf.
846 Central-proximal sections obtained using confocal imaging were collected and
847 quantified. Treatment with DMH4 inhibits laminin removal and results in optic fissure

848 fusion failure. Scale bar = 50um. **C)** Quantification of laminin signal intensity within the
849 optic fissure, normalized to regions of laminin staining juxtaposed to the lens. Relative
850 pixel intensities are displayed. A green dotted line depicts the trend in laminin intensity
851 over time, a blue dotted line represents the WT trend. ANOVA $p<0.0001$. **D)**
852 Quantification of F-actin signal intensity (phalloidin staining) within the optic fissure,
853 normalized to regions of F-actin signal within the lobe of the retina. Relative pixel
854 intensities are displayed. A red dotted line represents the trend in F-actin intensity over
855 time, a blue dotted line represents the WT trend. ANOVA $p<0.0001$.
856
857 Figure 6: **ADAMTS1 inhibits retinal vascularization.**
858 **A)** Wholemount in situ hybridization comparing ADAMTS1 expression between WT and
859 pax2a$^{-/-}$ embryos at 28 and 32hpf. ADAMTS1 signal within the optic fissure (yellow
860 arrowhead) is clearly increased in Pax2a$^{-/-}$ embryos (red *). **B)** Comparison of WT and
861 ADAMTS1 mRNA injected embryo vascularization during optic fissure fusion, 24-48hpf.
862 3D reconstructions of whole mount Tg[kdrl:mCherry] (red) WT or ADAMTS1 mRNA
863 injected embryos with DNA stained by DAPI (blue). Scale bar = 50um. **C)** Quantification
864 of mCherry positive cells from 3D confocal stacks within the region of the optic fissure.
865 Individual embryo results are depicted. * $p<0.001$, ANOVA $p<0.0001$. **D)** 3D
866 reconstruction of Tg[kdrl:mCherry] (red) WT or ADAMTS1 MO injected embryos at
867 48hpf. DNA is stained with DAPI (blue). Inhibiting ADAMTS1 function leads to
868 significant disorganization of the dorsal vasculature (yellow *) as well as misconnections
869 within the vascular network (yellow arrowhead). Scale bar = 50um.
870
871 Figure 7: **ADAMTS1 misregulation leads to failure of optic fissure fusion.**
872 **A)** Whole mount Immunohistochemistry was used to simultaneously visualize F-actin
873 (red) and laminin (green) during optic fissure fusion, 24-72hpf in ADAMTS1 mRNA
874 injected embryos. Central-proximal sections obtained using confocal imaging were
875 collected and quantified. Scale bar = 50um. **B)** Quantification of laminin signal intensity
876 within the optic fissure, normalized to regions of laminin staining juxtaposed to the lens.
877 Relative pixel intensities are displayed. A green dotted line depicts the trend in laminin
878 intensity over time, blue line depicts WT trends. ANOVA $p<0.0001$. **C)** Quantification of

F-actin signal intensity (phalloidin staining) within the optic fissure, normalized to regions of F-actin signal within the lobe of the retina. Relative pixel intensities are displayed. A red dotted line represents the trend in F-actin intensity over time, blue line represents WT trends. ANOVA $p<0.0001$.

889 **Supplemental Material**

890

891 Figure S1: **Optic Fissure quantification strategy**

892 **A**) Graphical representation of the region of OF analyzed using confocal microscopy. **B**)
893 Sample image depicting regions of the OF (1), laminin normalization (2) and f-actin
894 normalization (3) used for signal intensity quantification.

895

896 Figure S2: **Optic Fissure apposition measurements.**

897 Measurements of the distance between retinal lobes (apposition) in WT, pax2a$^{-/-}$, DMH4
898 treated or ADAMTS1 mRNA injected embryos at 48hpf. Measurements were made
899 using laminin staining as reference for edges of retinal lobes. Distance was measured
900 as pixels.

901

902 Figure S3: ***pax2a* and *tln1* expression during development**

903 **A**) Whole mount in situ hybridization of pax2a probe at 24, 48, 54 and 72hpf. Lateral
904 (top) and ventral (bottom) images depicting optic fissure expression are shown. Pax2a
905 expression persists in the fissure up to 54hpf. **B**) Whole mount in situ hybridization of
906 tln1 probe at 24, 48, 54 and 72hpf. Lateral (top) and ventral (bottom) images depicting
907 optic fissure expression are shown. Tln1 expression is detected in the optic fissure from
908 24-48hpf (yellow arrowheads).

909

910 Figure S4: **DMH4 dose response**

911 3D reconstructions of 48hpf whole mount Tg[kdrl:mCherry] (red) embryos treated with 1,
912 5, 50 or 100uM DMH4. DNA stained with DAPI (blue). Increasing concentration of
913 DMH4 eliminates mCherry expressing cells from the optic fissure and retina. Scale bar
914 = 50um.

915

916 Movie 1: WT Tg[kdrl:mCherry] migration within the optic fissure, 24-30hpf

917

918 Movie 2: pax2a$^{-/-}$ Tg[kdrl:mCherry] migration within the optic fissure, 24-30hpf

919

920 Movie 3: 3D rotation of WT Tg[kdrl:mCherry] embryo at 48hpf

921

922 Movie 4: 3D rotation of pax2a$^{-/-}$ Tg[kdrl:mCherry] embryo at 48hpf

923

924 Movie 5: 3D rotation of 48hpf Tg[kdrl:mCherry] embryo injected with ADAMTS1 mRNA

925

926 Movie 6: 3D rotation of 48hpf Tg[kdrl:mCherry] embryo injected with ADAMTS1

927 morpholino

928

929 Table 1: pax2$^{-/-}$ 48hpf retinal expression changes.

Figure 1

A

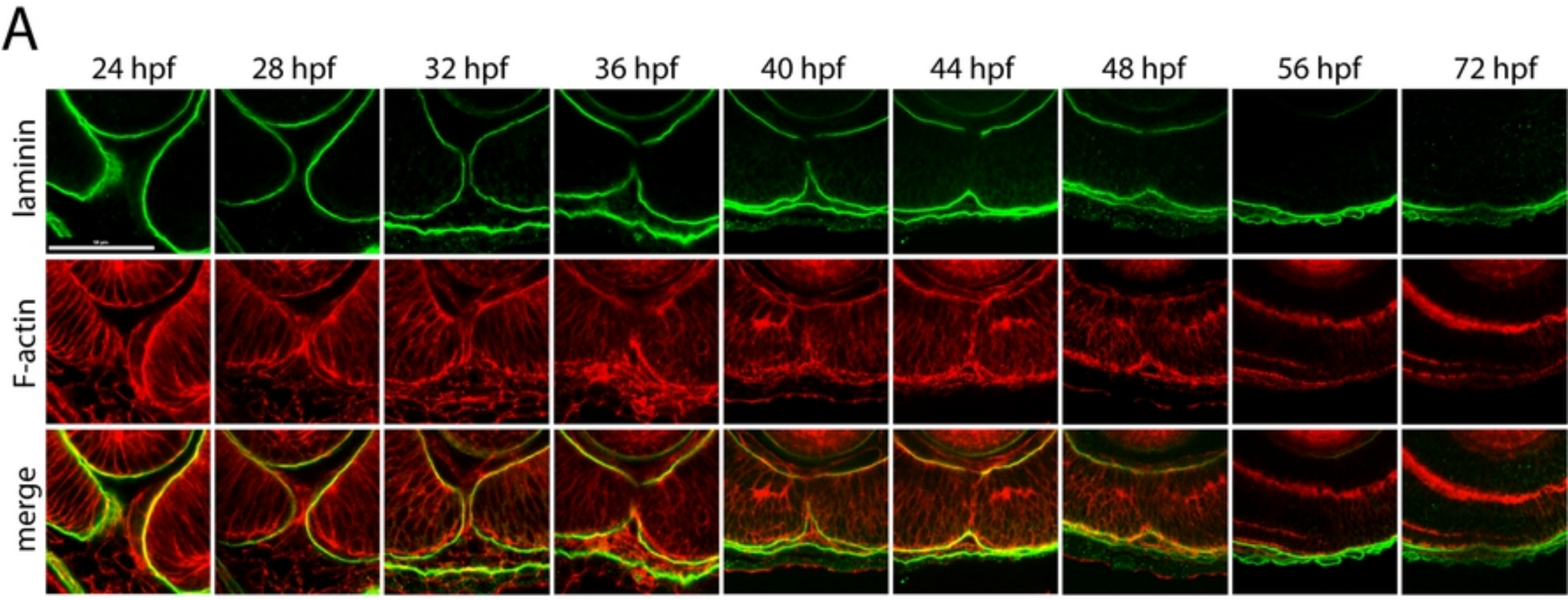
24 hpf
28 hpf
32 hpf
36 hpf
40 hpf
44 hpf
48 hpf
56 hpf
72 hpf
laminin
F-actin
merge

B

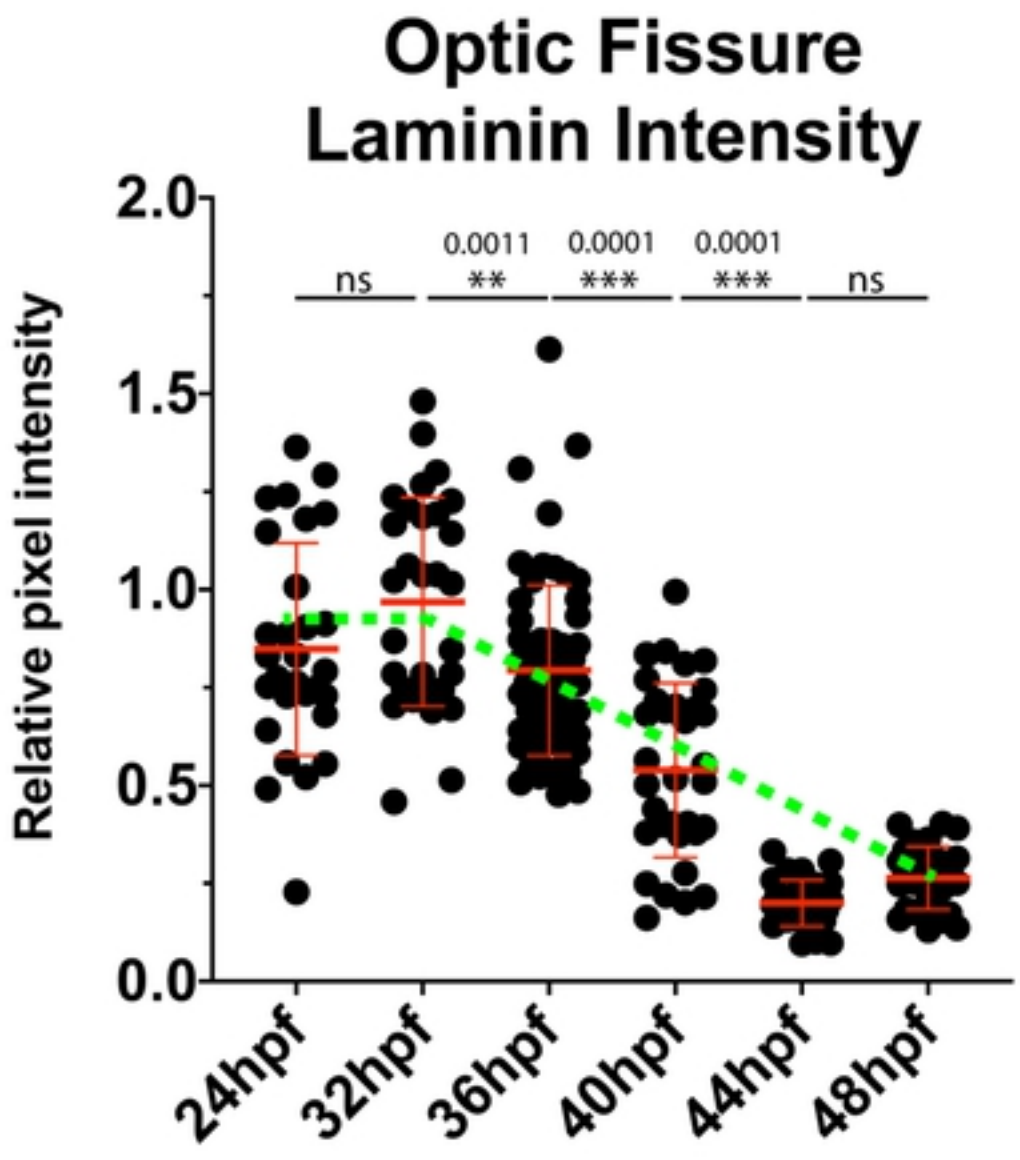
Optic Fissure
Laminin Intensity
Relative pixel intensity
2.0
1.5
1.0
0.5
0.0
ns
0.0011
**
0.0001
***
0.0001
***
ns
24hpf
32hpf
36hpf
40hpf
44hpf
48hpf

C

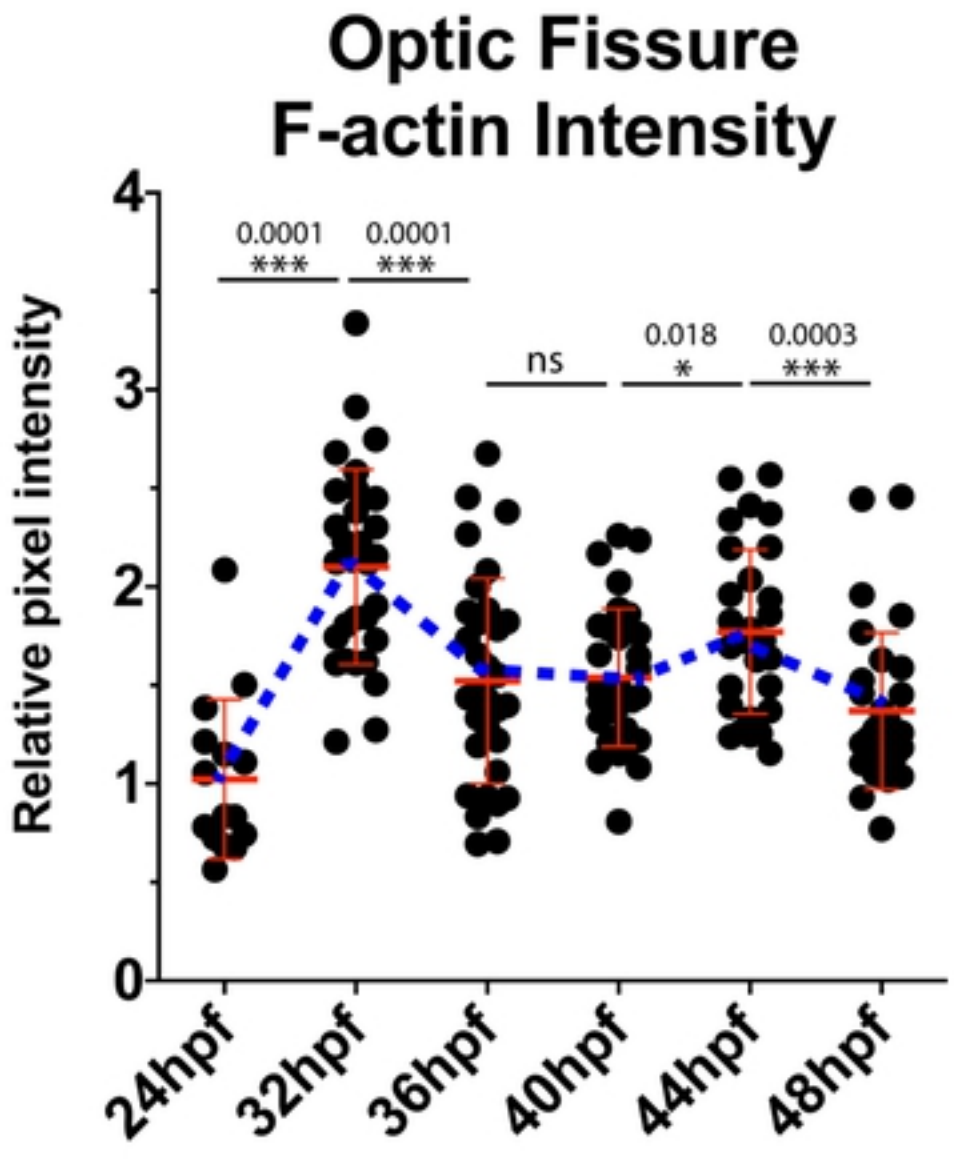
Optic Fissure
F-actin Intensity
Relative pixel intensity
4
3
2
1
0
0.0001
***
0.0001
***
ns
0.018
*
0.0003
***
24hpf
32hpf
36hpf
40hpf
44hpf
48hpf

Figure 2

A

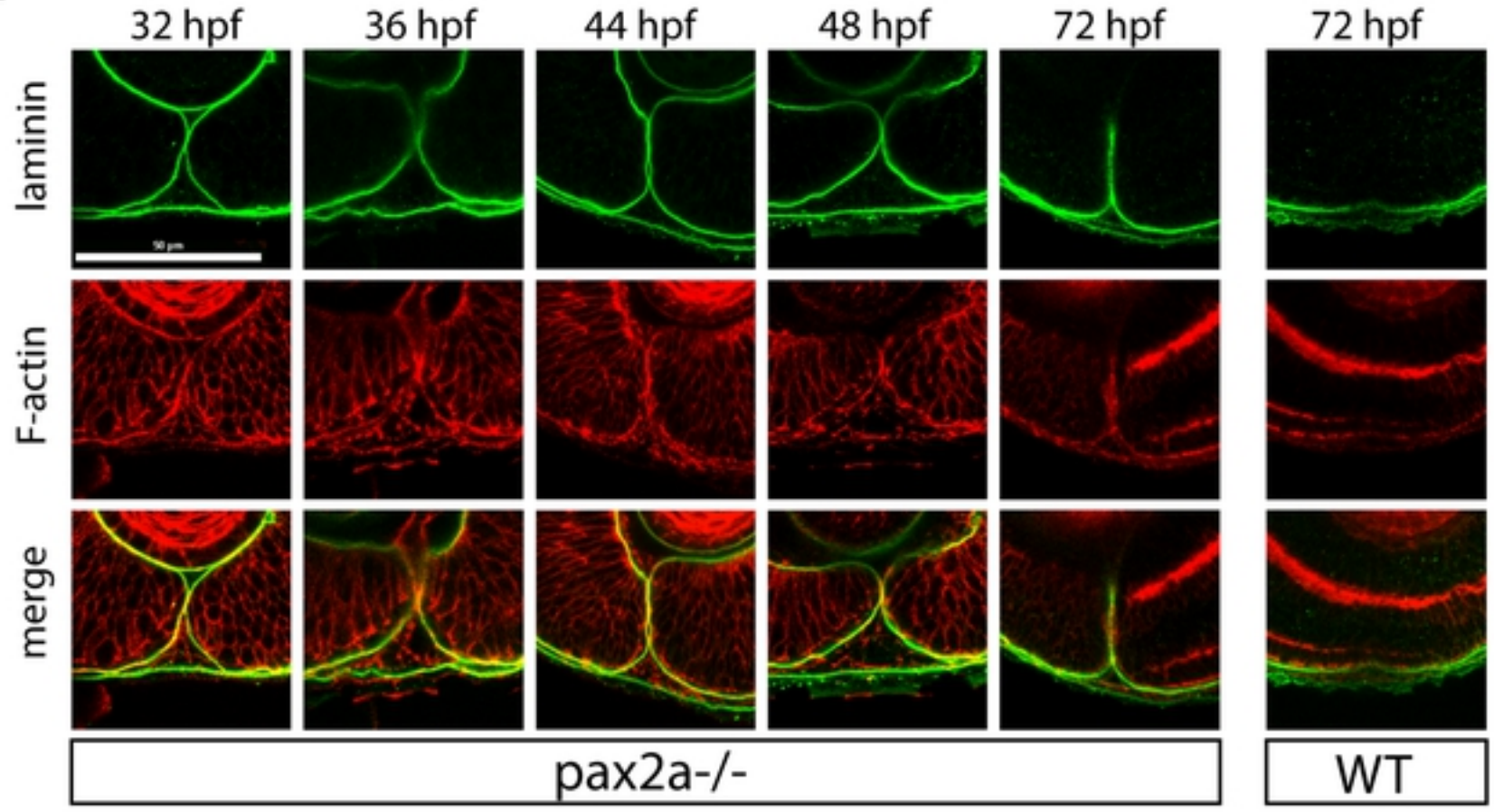
32 hpf
36 hpf
44 hpf
48 hpf
72 hpf
72 hpf
laminin
F-actin
merge
pax2a-/-
WT

B

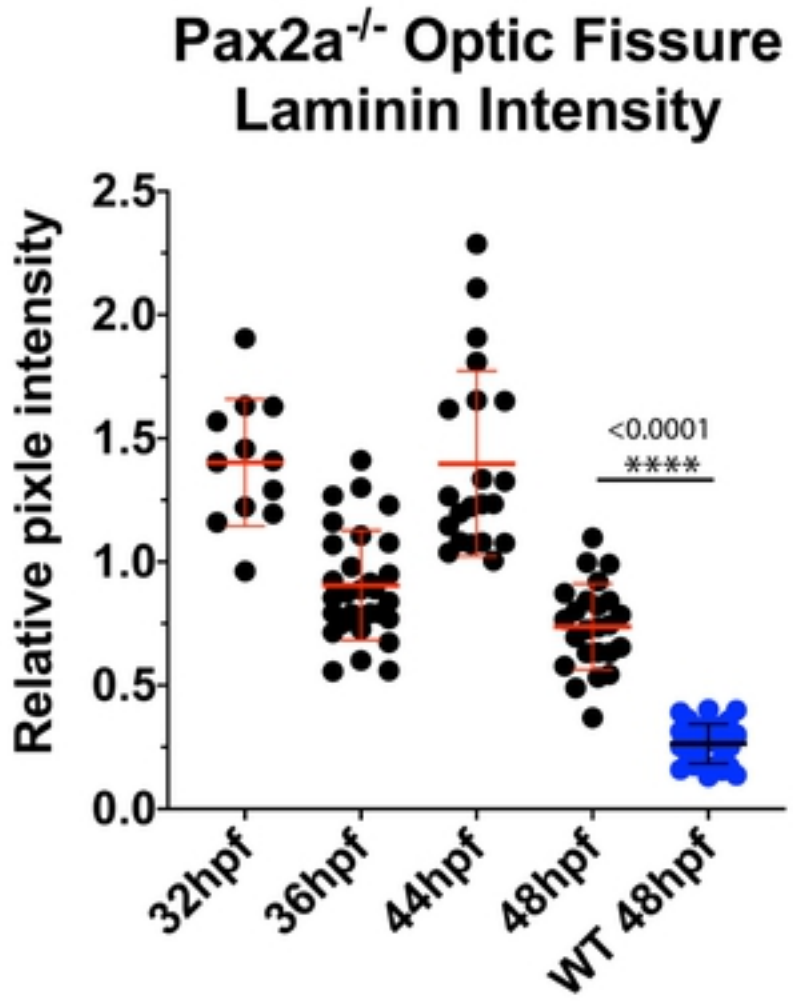
Pax2a-/- Optic Fissure
Laminin Intensity
Relative pixle intensity
2.5
2.0
1.5
1.0
0.5
0.0
<0.0001
****
32hpf
36hpf
44hpf
48hpf
WT 48hpf

C

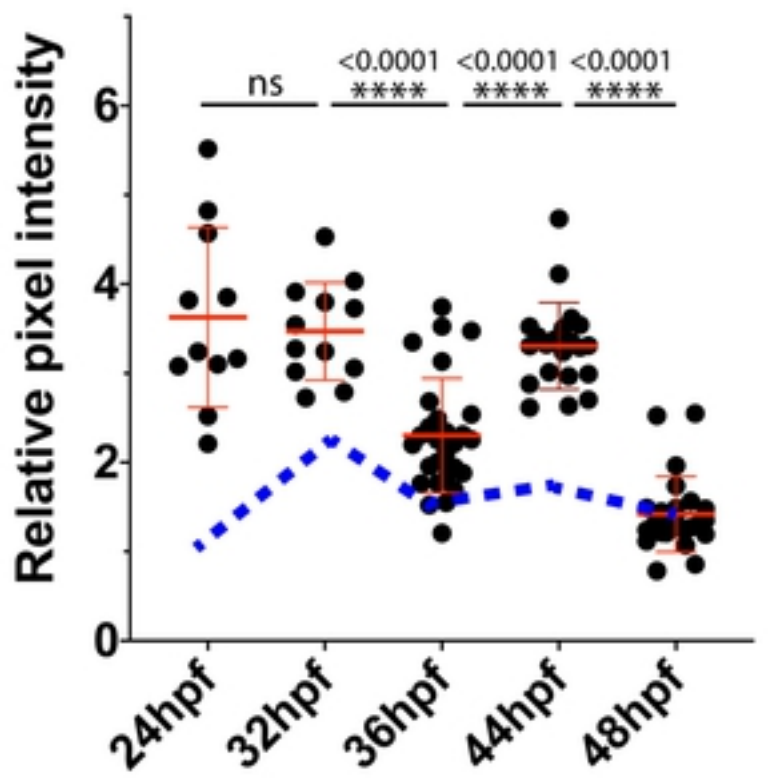
Pax2a-/- Optic Fissure
F-actin Intensity
Relative pixel intensity
6
4
2
0
ns
<0.0001
****
<0.0001
****
<0.0001
****
24hpf
32hpf
36hpf
44hpf
48hpf

Figure 3

A

B

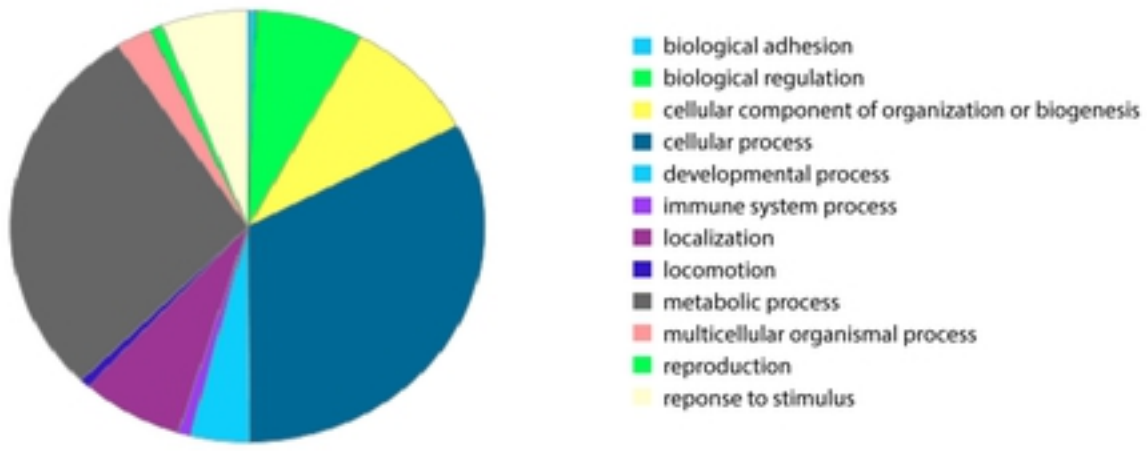

C

Gene ID	Gene Name	GO Term
aifm1	Apoptosis-inducing factor, mitochondrion-associated 1	oxidoreductase activity
sumo3a	small ubiquitin-like modifier 3a	protein sumoylation
lim2.1	Lens intrinsic membrane protein 2.1	Membrane
tfb2m	transcription factor B2, mitochondrial	transferase activity
tln1	Talin 1	actin binding
mgst2	microsomal glutathione S-transferase 2	enzyme activator activity
si:ch211-57b15.1	si:ch211-57b15.1	NA
ptprna	protein tyrosine phosphatase, receptor type, Na	protein dephosphorylation
dnajb11	DnaJ (Hsp40) homolog, subfamily B, member 11	protein folding
krt96	Keratin 96	structural molecule activity
sept9a	septin 9a	GTP binding
si:rp71-36a1.5	si:rp71-36a1.5	membrane
si:dkey-9c18.3	si:dkey-9c18.3	NA
arf5	ADP Ribosylation Factor 5	GTP binding
dock1	Dedicator Of Cytokinesis 1	small GTPase mediated signal transduction
hbbe1.1	Embryonic 1 beta-globin	Hemoglobin Complex
zgc:152951	Zgc:152951	electron transfer activity
pcbp3	Poly(rC)-binding protein 3	RNA binding
gpsm1b	G protein-signaling modulator 1b	GTPase regulator activity
abracl	Costars family protein ABRACL	regulation of actin filament-based process

D

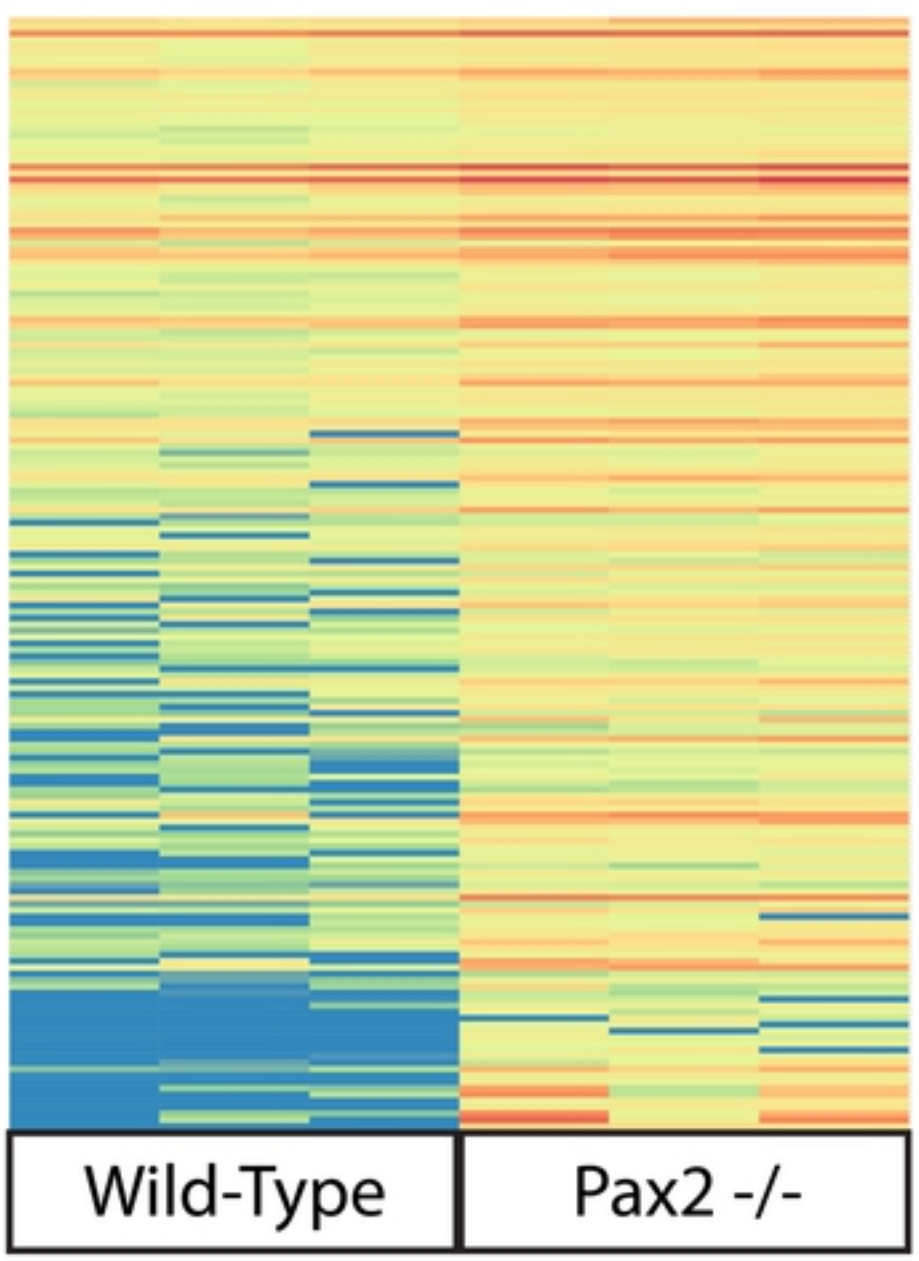

E

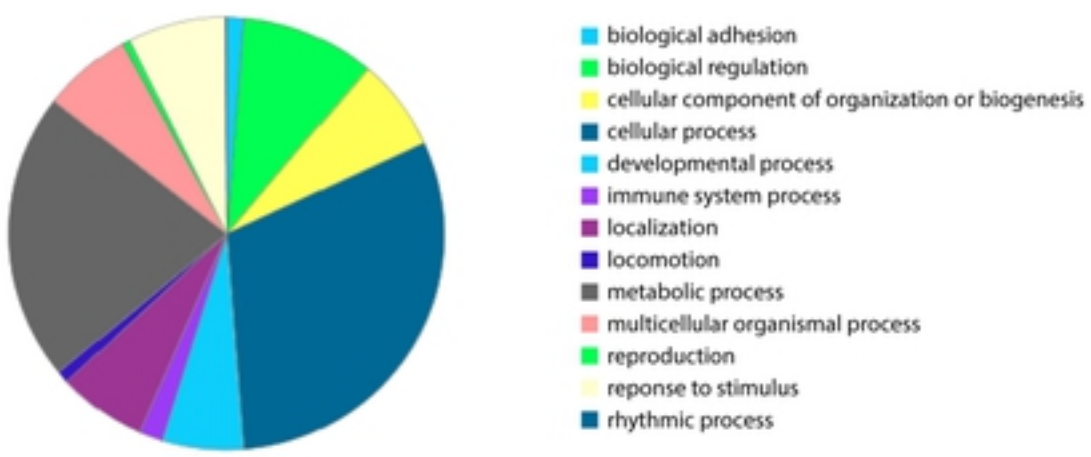

F

Gene ID	Gene Name	GO Term
gmnn	geminin, DNA replication inhibitor	regulation of DNA replication
col11a1a	collagen, type XI, alpha 1a	extracellular matrix structural constituent
fubp3	far upstream element (FUSE) binding protein 3	RNA binding
si:dkey-26g8.4	Cathepsin Lb	proteolysis
ublcp1	ubiquitin-like domain containing CTD phosphatase 1	protein dephosphorylation
smarcal1	SWI/SNF related, matrix, actin dependent regulator of chromatin, a-like 1	DNA repair
he1b	hatching enzyme 1b	metalloendopeptidase activity
anxa3a	annexin A3a	regulation of NMDA receptor activity
si:dkey-269i1.4	cathepsin L1-like	proteolysis
zgc:174855	zgc:174855	
gsta.1	glutathione S-transferase, alpha tandem duplicate 1	glutathione metabolic process
tbc1d7	TBC1 domain family, member 7	activation of GTPase activity
srek1	splicing regulatory glutamine/lysine-rich protein 1	regulation of alternative mRNA splicing
scg5	secretogranin V	neuropeptide signaling pathway
ggact.3	gamma-glutamylamine cyclotransferase, tandem duplicate 3	lyase activity
si:dkey-26g8.4	Cathepsin L1-like	proteolysis
si:dkey-239j18.3	si:dkey-239j18.3	proteolysis
ahsa1a	AHA1, activator of heat shock protein ATPase homolog 1a	ATPase activator activity
he1a	hatching enzyme 1a	metalloendopeptidase activity
dpf3	D4, zinc and double PHD fingers, family 3	zinc ion binding

Figure 4

A

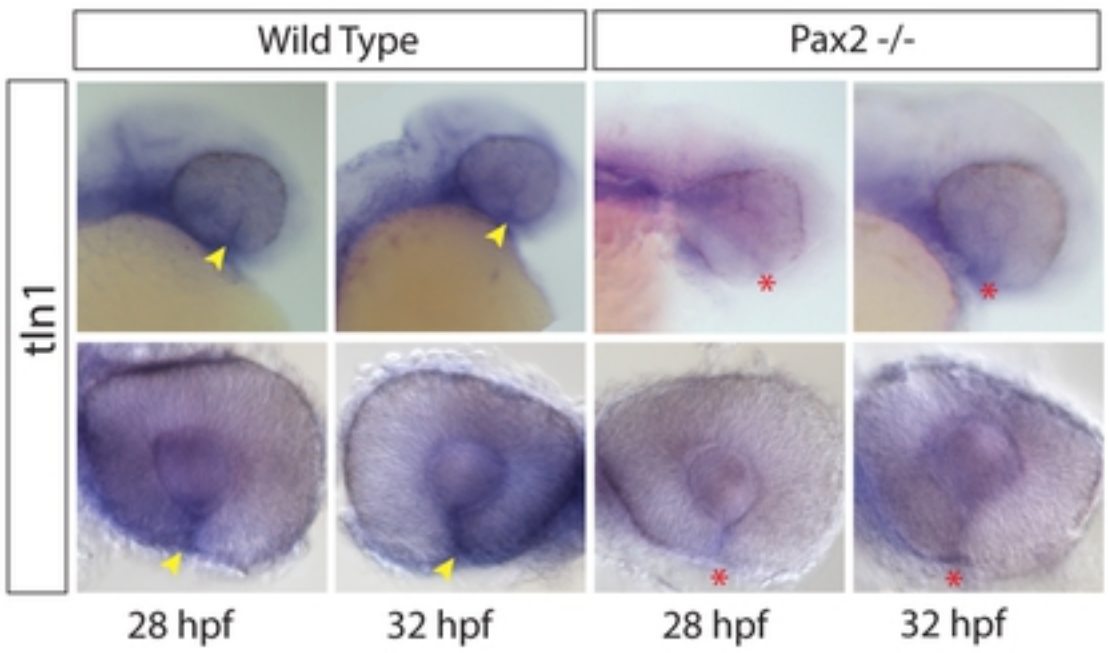

B

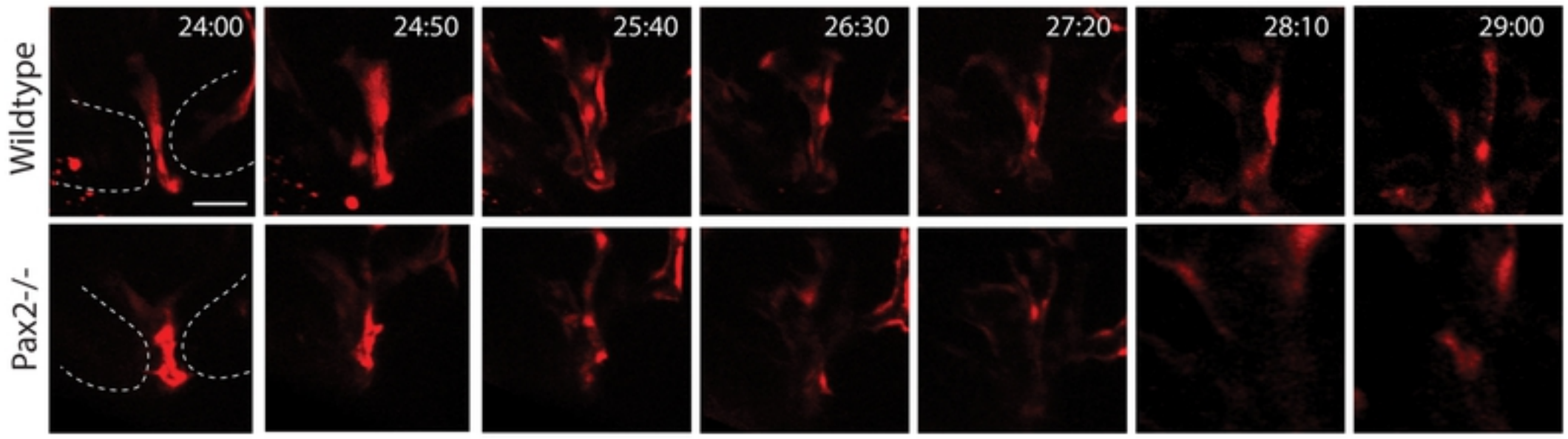

C

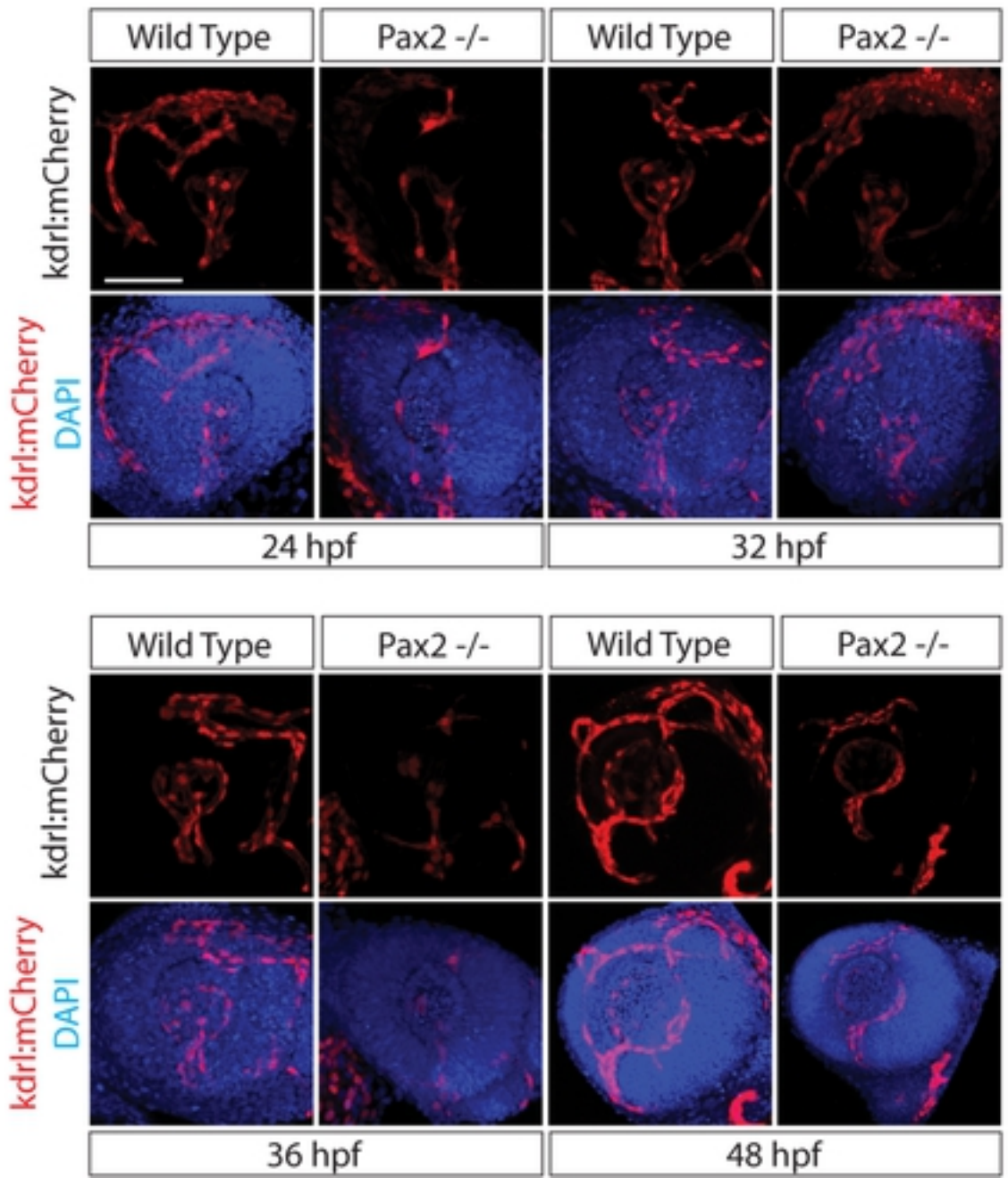

D

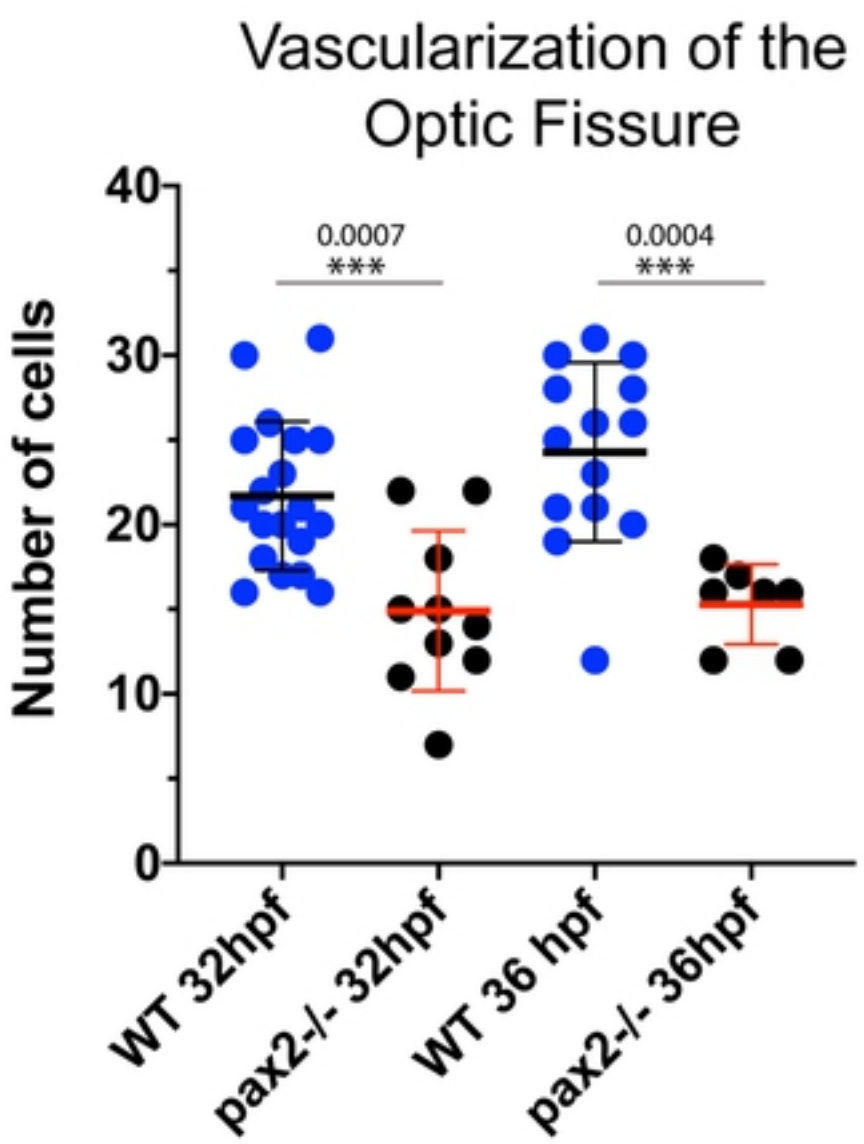

Figure 5

A

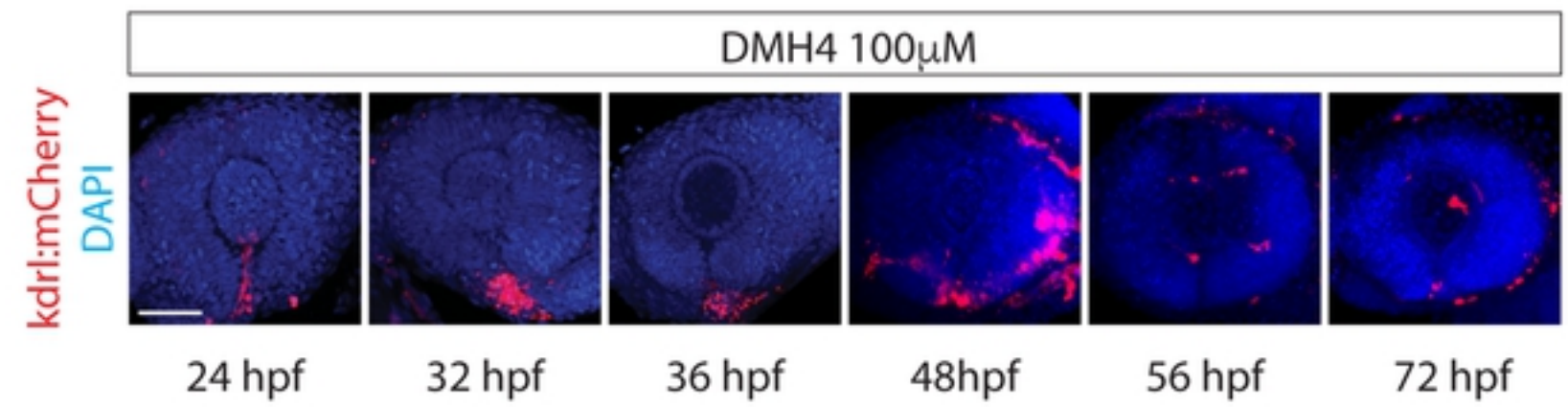

B

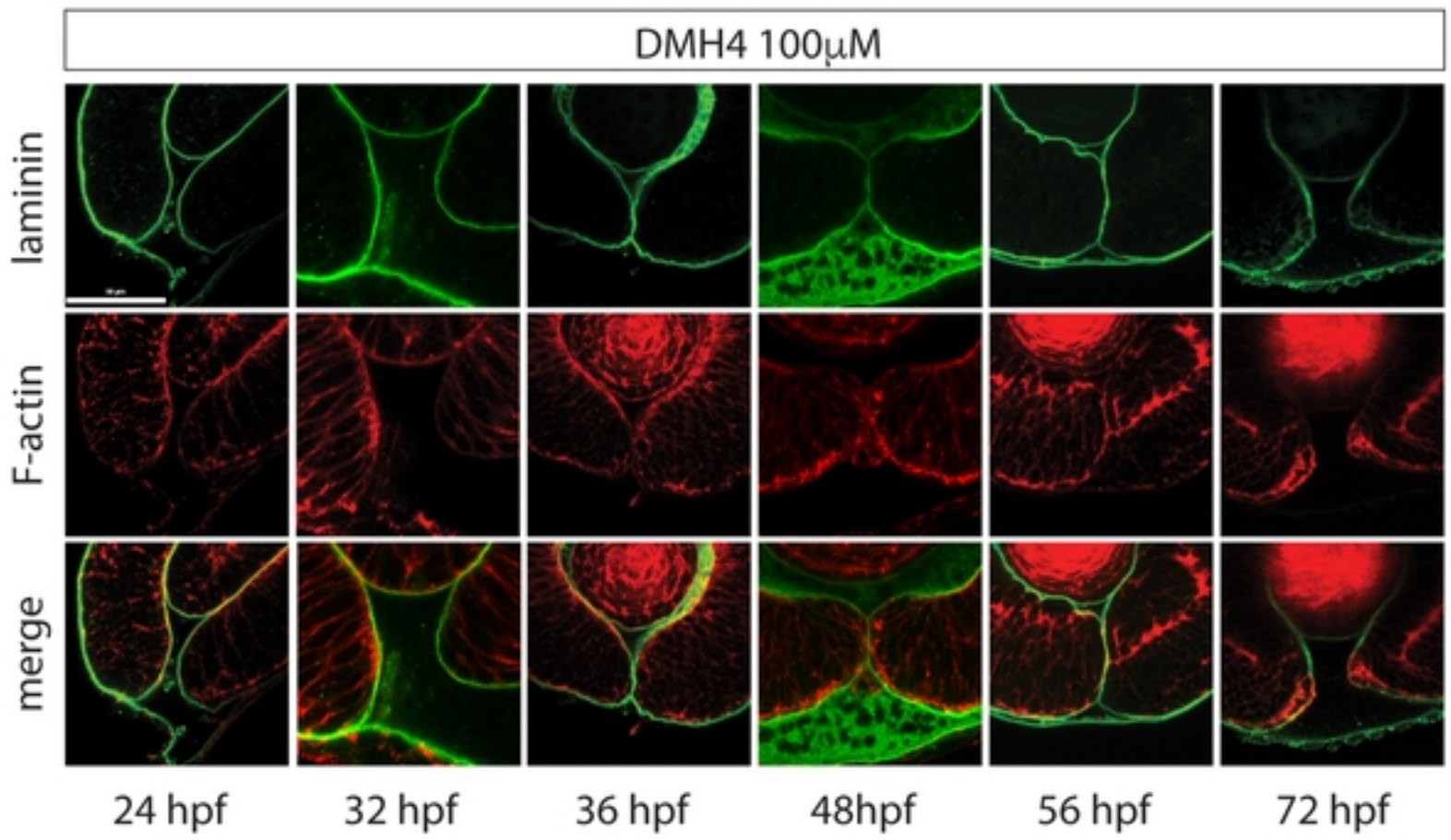

C

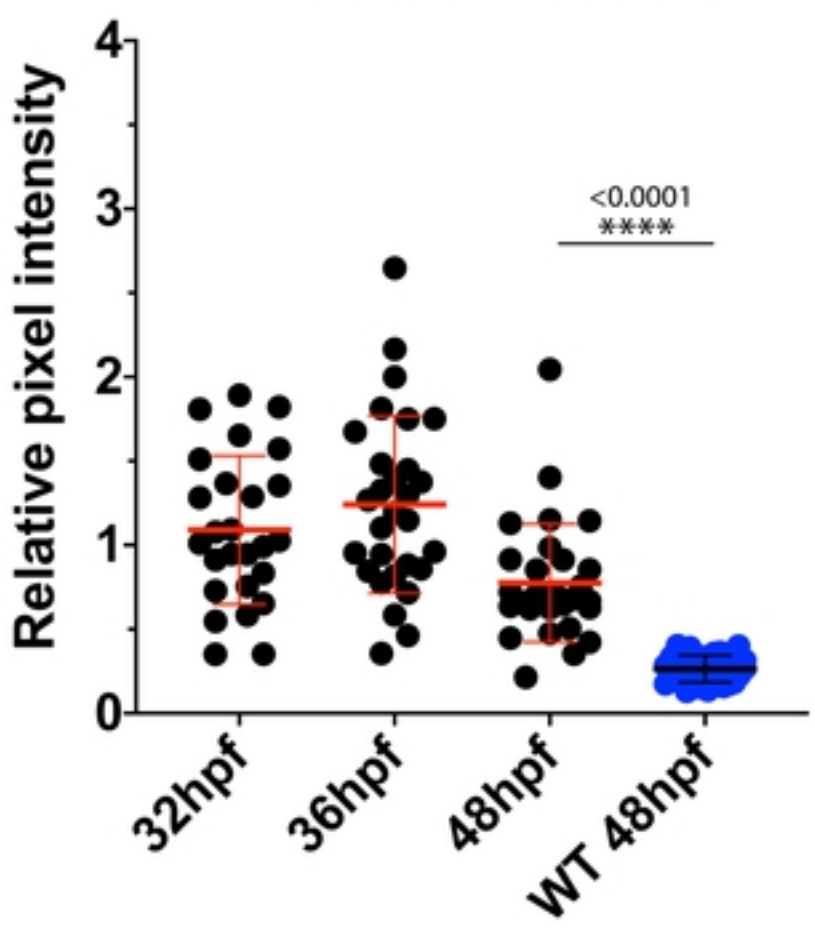

D

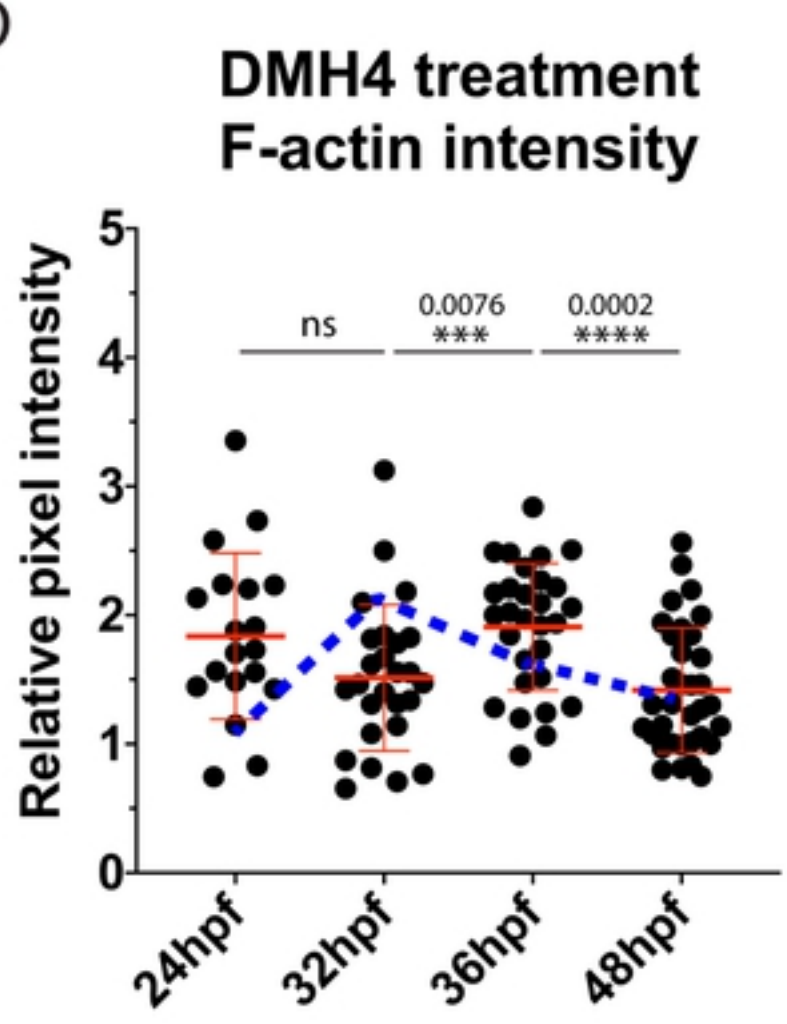

Figure 6

A

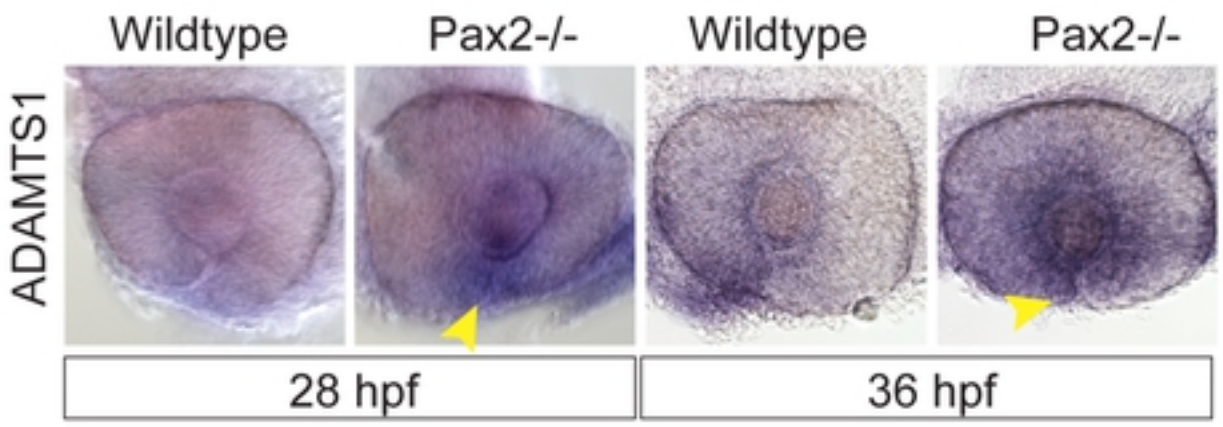

B

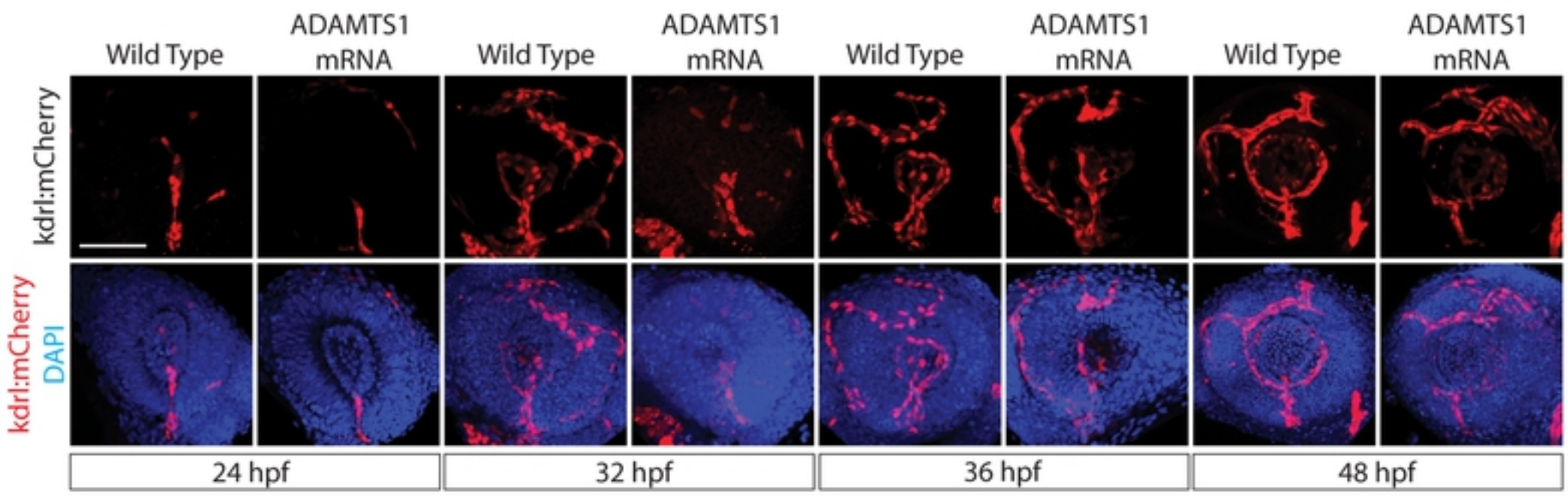

C

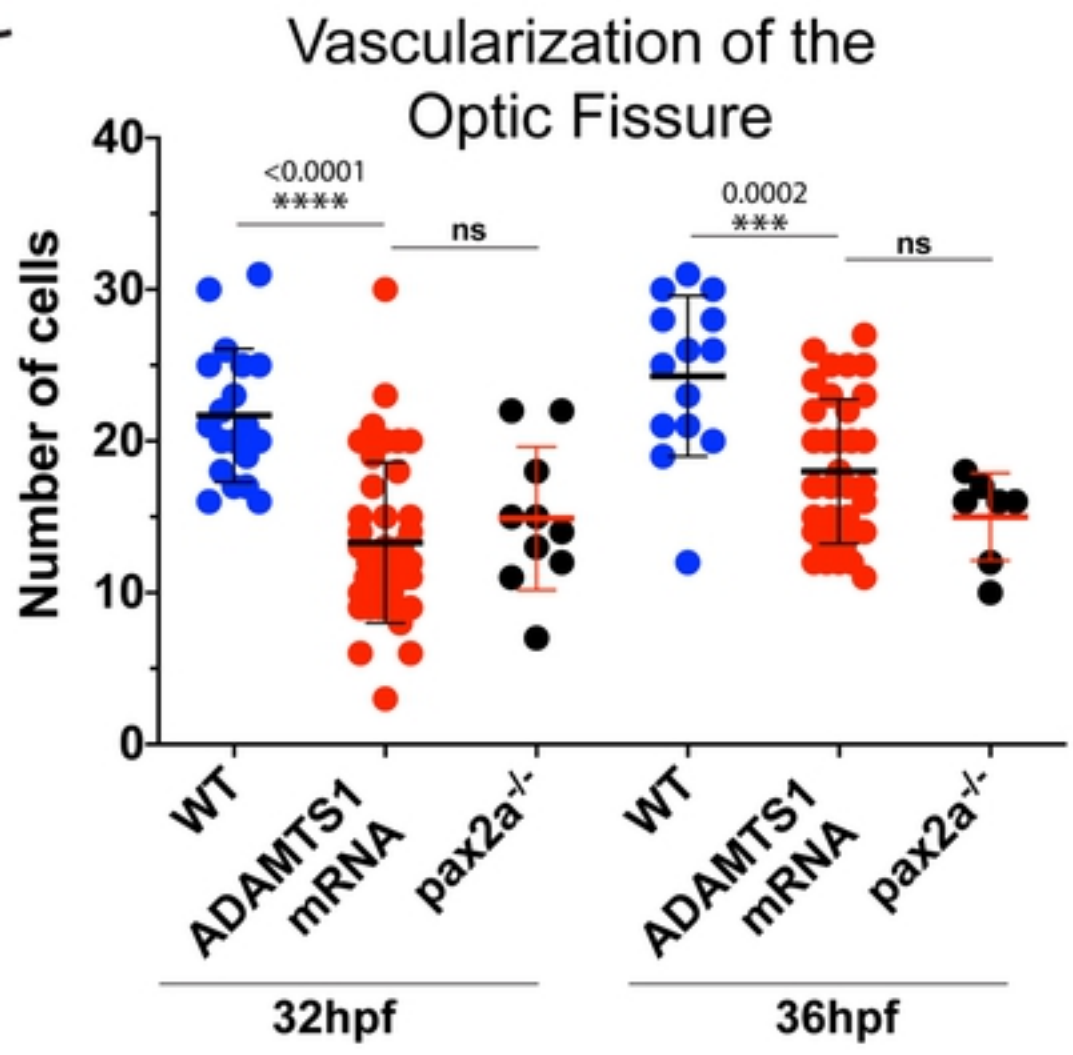

D

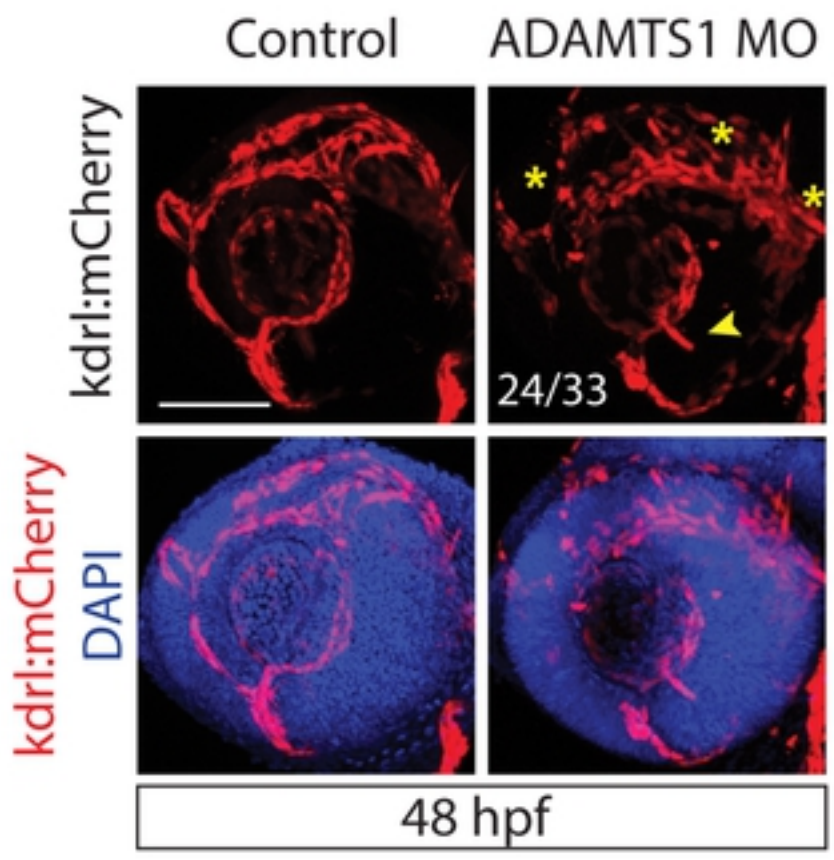

Figure 7

A

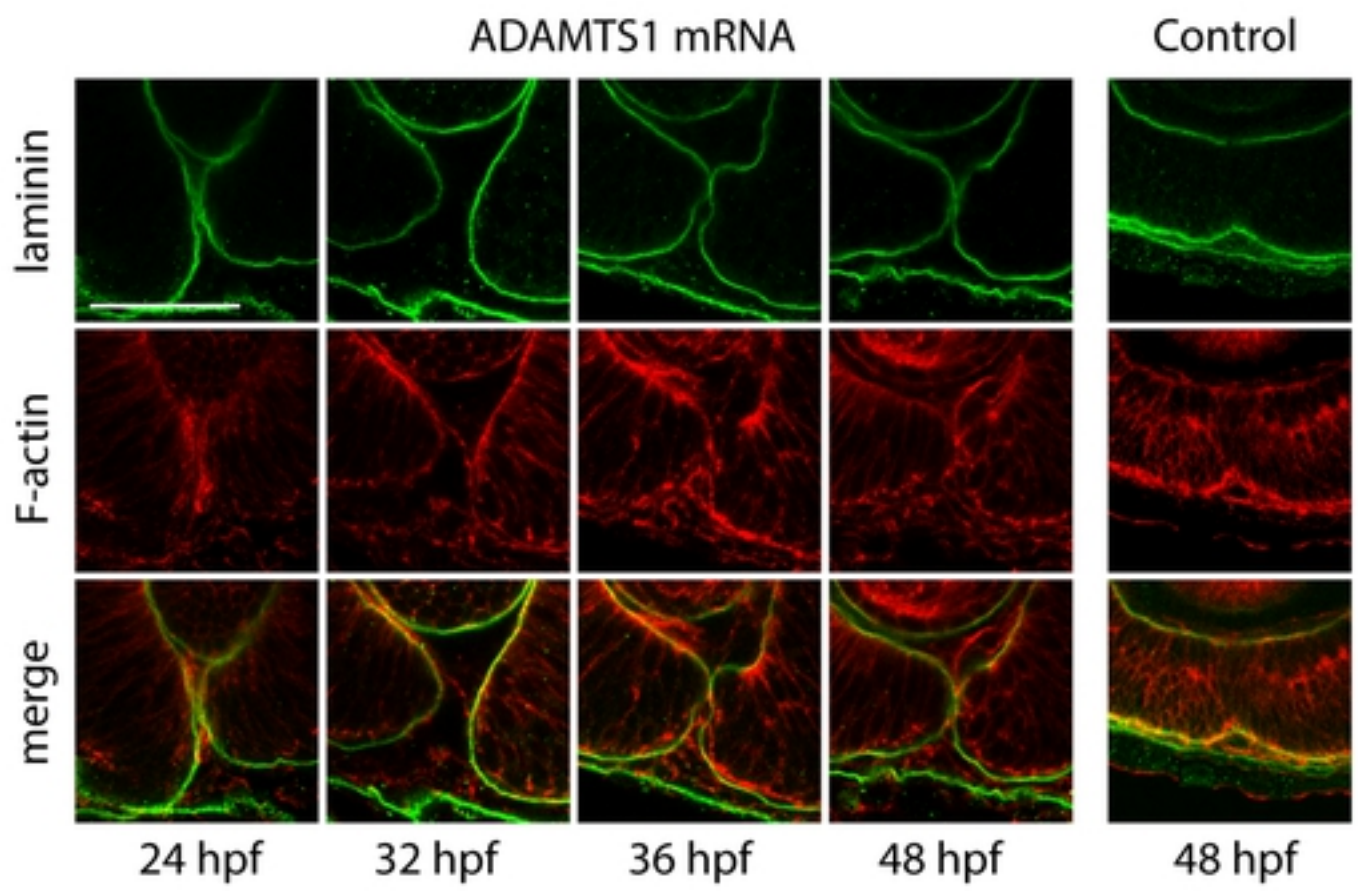
ADAMTS1 mRNA
Control
laminin
F-actin
merge
24 hpf
32 hpf
36 hpf
48 hpf
48 hpf

B

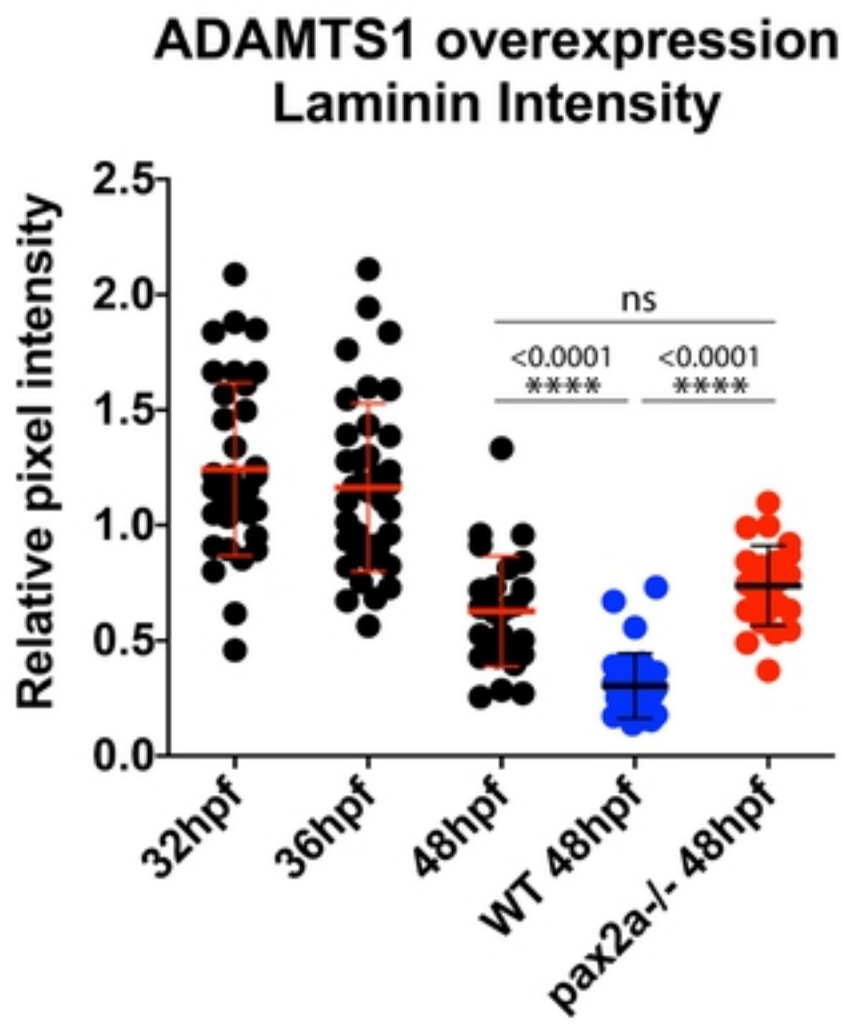
ADAMTS1 overexpression
Laminin Intensity
Relative pixel intensity
2.5
2.0
1.5
1.0
0.5
0.0
ns
<0.0001
****
<0.0001
****
32hpf
36hpf
48hpf
WT 48hpf
pax2a-/- 48hpf

C

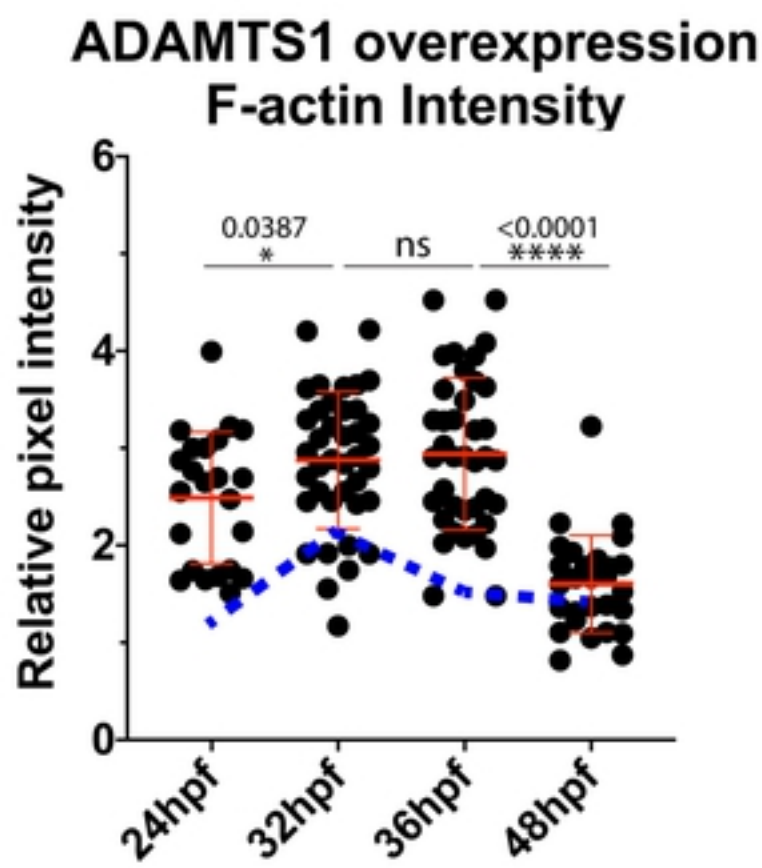
ADAMTS1 overexpression
F-actin Intensity
Relative pixel intensity
6
4
2
0
0.0387
*
ns
<0.0001
****
24hpf
32hpf
36hpf
48hpf

Supplementary Figure 1

A

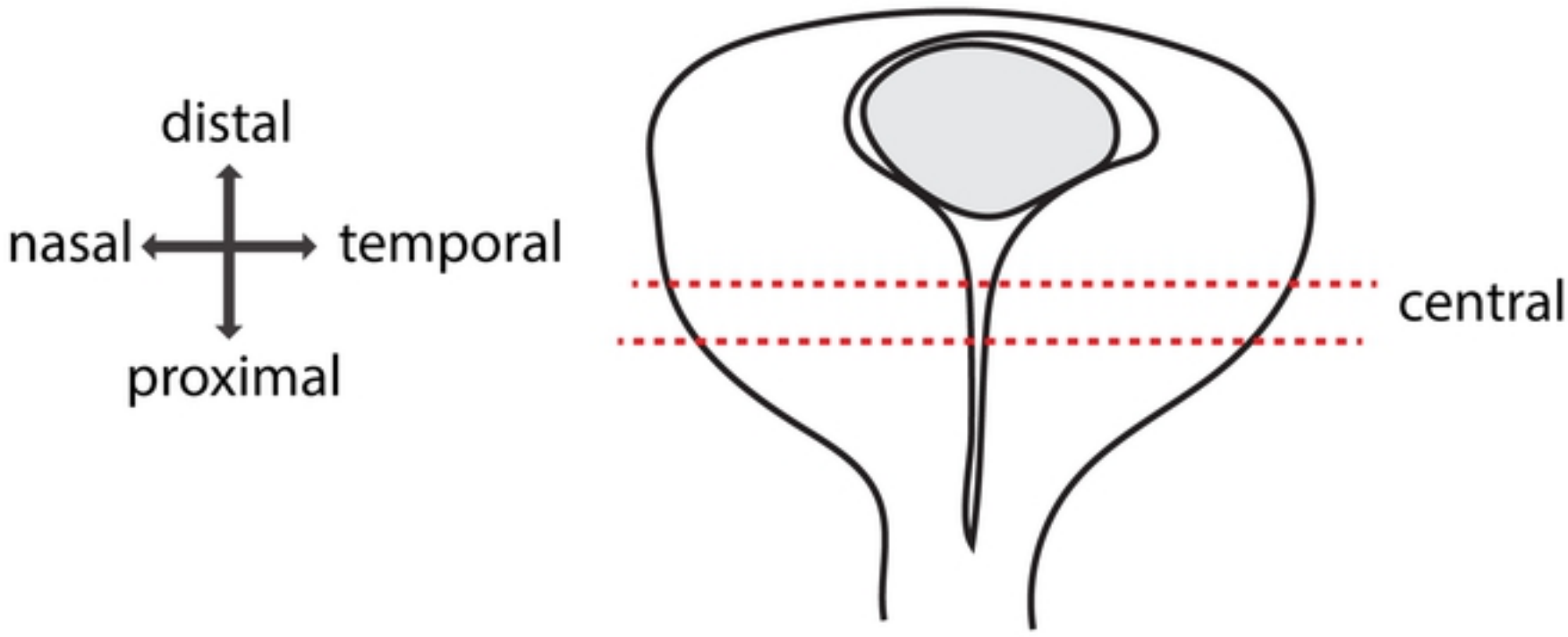

B

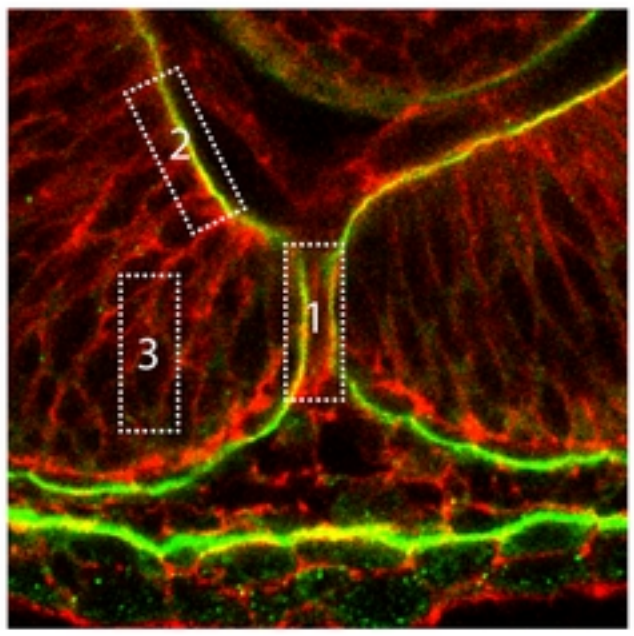

1: Optic Fissure Signal

2: Laminin signal normalization

3: Phalloidin (F-actin) signal normalization

Supplementary figure 2

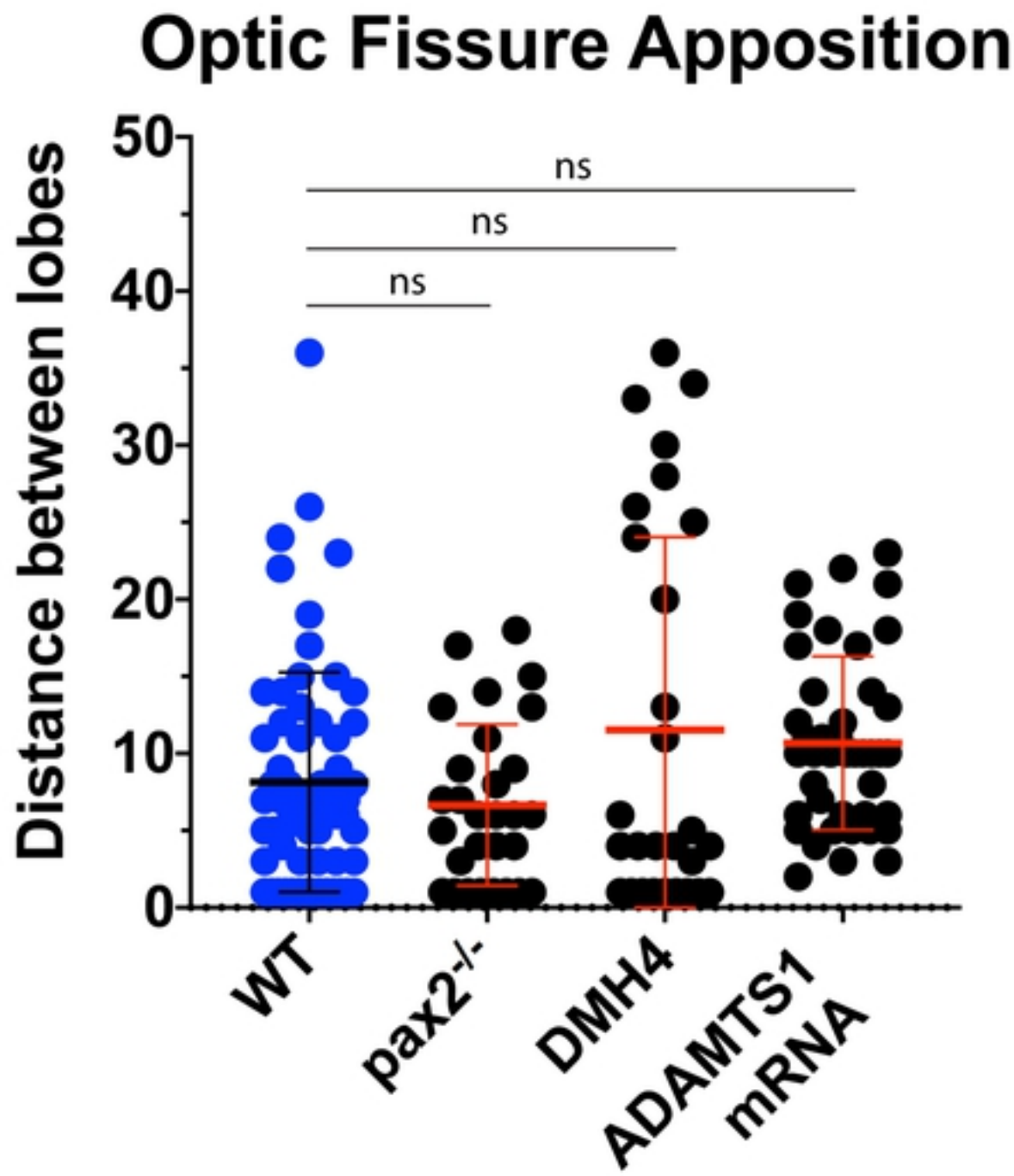

Supplementary Figure 3

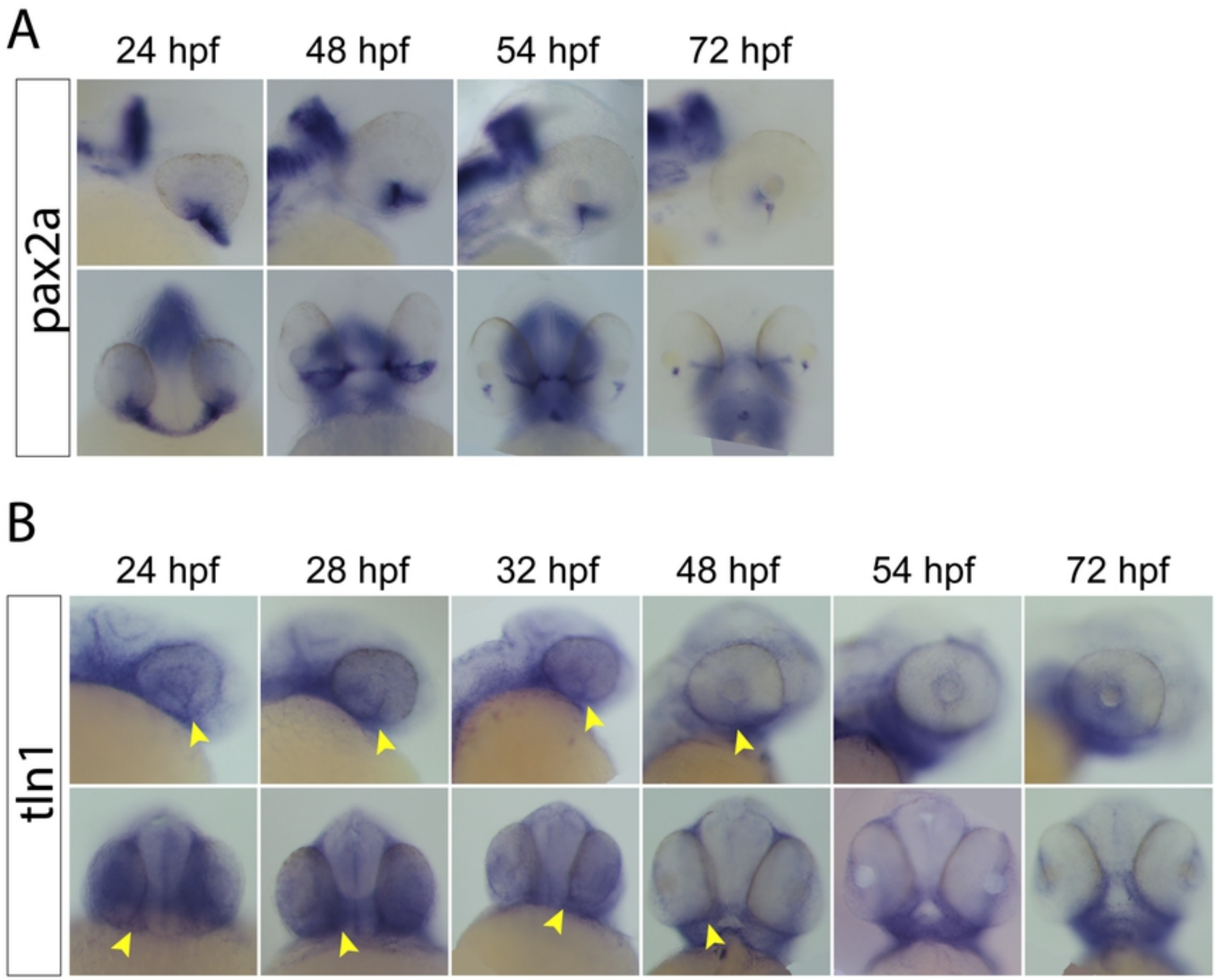
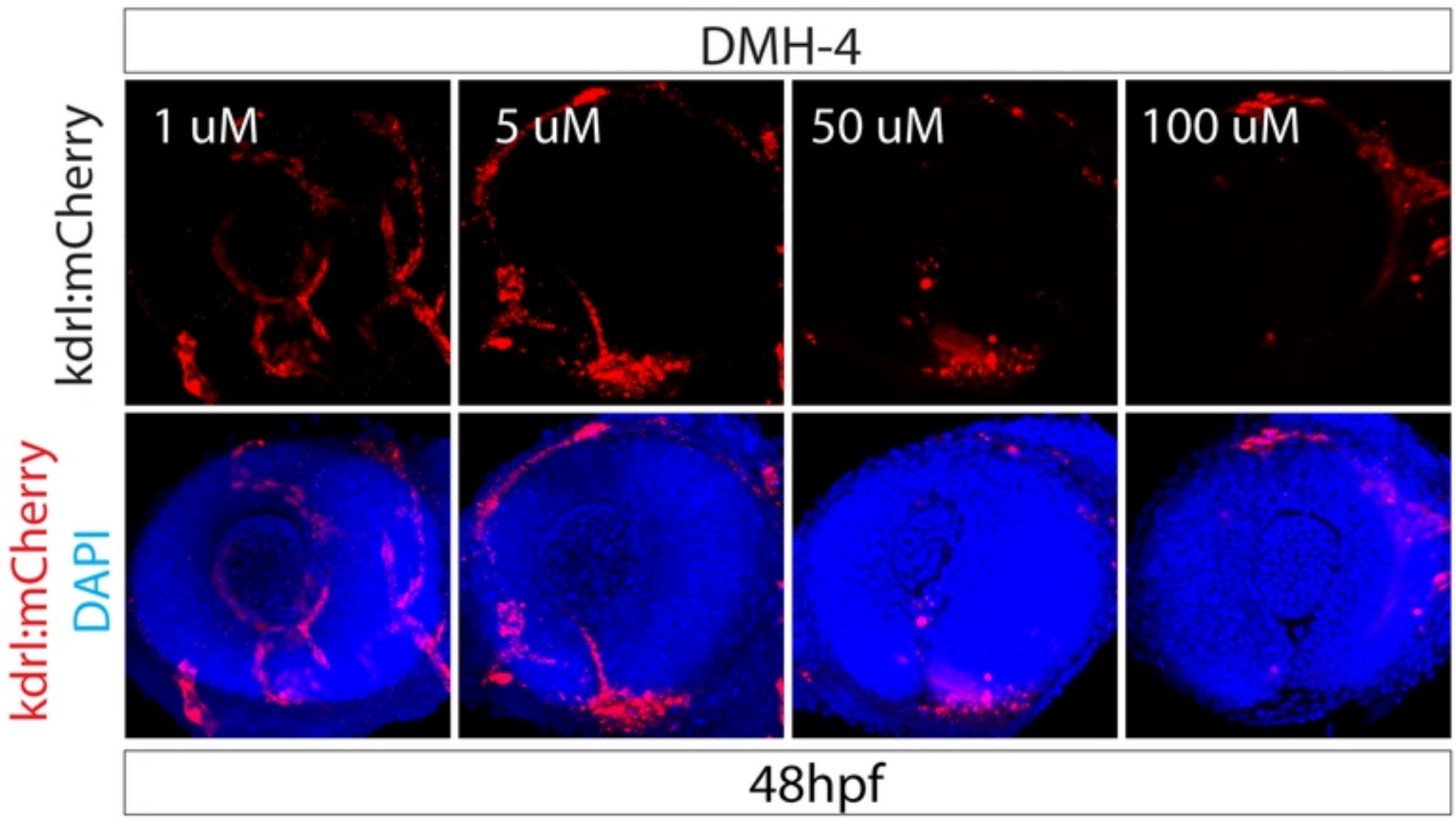
Supplementary Figure 4